KTH Royal Insistute of Technology

School of Engineering Sciences in Chemistry, Biotechnology and Health

Master thesis:
Simulation of dry matter loss in biomass storage

Date: 2019-06-24

Author: Jens Bjervås[1], bjervas@kth.se

Supervisors: Matthäus Bäbler[2], Erik Dahlen[3]

[1]Master student at the department of Chemical Engineering, KTH
[2]Associate professor at the department of Chemical Engineering, KTH
[3]Research and development manager at Stockholm Exergi

Contents

Foreword

I would like to begin this report by giving a big thanks to Matthäus Bäbler, Erik Dahlen and Erik Anerud for their support and invaluable contribution to the project.

Abstract

Material degradation and a decrease of fuel quality are common phenomena when storing biomass. A Magnitude of 7.8% has been reported to degrade over five months when storing spruce wood chips in the winter in Central Europe. This thesis presents a theoretical study of biomass storage. It includes investigations of bio-chemical, chemical and physical processes that occur during storage of chipped woody biomass. These processes lead to degradation caused by micro-activity, chemical oxidation reactions and physical transformation of water. Micro-activity was modeled with Monod kinetics which are Michaelis-Menten type of expressions. The rate expressions were complemented with dependency functions describing the impact of oxygen, moisture and temperature. The woody biomass was divided into three fractions. These fractions represent how hard different components of the wood are to degrade by microorganisms. Chemical oxidation was modeled as a first order rate expression with respect to the active components of the wood. Two different cases have been simulated during the project. Firstly, an isolated system with an initial oxygen concentration of air was considered. This case displayed a temperature increase of approximately $2°C$ and a material degradation less than 1%. The second case considered an isolated system with an endless depot of oxygen. This case resulted in degradation losses around 0.45-0.95% in the temperature range between 65-80$°C$ during approximately 300 days of storage. The temperature increased slowly due to chemical oxidation.

Nomenclature

Table 1: Quantities, descriptions and units used in the simulations.

Quantity	Description	Unit
ρ	Density	kg/m^3
ρ_{S_H}	Hard to degrade fraction of substrate (makro-molecules)	kg/m^3
ρ_{S_E}	Easy to degrade fraction of substrate (extractives)	kg/m^3
ρ_{S_I}	Inert fraction of substrate	kg/m^3
ρ_m	Active microorganisms	kg/m^3
ρ_d	Dead microorganisms	kg/m^3
ρ_{O_2}	Oxygen	kg/m^3
ρ_{CO_2}	Carbon dioxide	kg/m^3
ρ_{N_2}	Nitrogen	kg/m^3
$\rho_{(W,L)}$	Liquid water	kg/m^3
$\rho_{(W,V)}$	Water vapor	kg/m^3
M	Molecular weight	g/mole
c_p	Specific heating value	kJ/(kg $\cdot$ K)
ΔH	Specific entalphy	kJ/kg
p	Pressure	Pa
T	Temperature	K
R	Gas constant	J/(mole $\cdot$ K)
r	Reaction rate	kg/(m$^3 \cdot$ s)
α	Weight fraction in bio-chemical reaction path	-
k_1	Rate constant	s^{-1}
K_{S_1}	Saturation constant	-
k_2	Rate constant	s^{-1}
K_{S_2}	Saturation constant	kg/m^3
k_3	Rate constant	s^{-1}
ω	Weight fraction	-
ν	Stoichiometric coefficient	-
k_0	Pre-exponential factor	s^{-1}
E_A	Activation energy	J/mole
A	Antoine constant	-
B	Antoine constant	-
C	Antoine constant	-
f	Conversion factor	(kg $\cdot$ Pa)/(g $\cdot$ mmHg)
$\dot{S}$	Heat source	kJ/(m$^3 \cdot$ s)
Q	Heat transport	kJ/(m$^3 \cdot$ s)
D	Diffusion coefficient	m^2/s
μ	Dynamic viscosity	Pa $\cdot$ s
β	Permeability coefficient	m^2

Chapter 1 - Scope and aims

1.1 Aim

The aim of this thesis was to develop a mathematical model to predict dry matter losses related to large-scale storage of chipped woody biomass. The total material loss is the sum of biological degradation, chemical oxidation and physical transformation e.g. condensation and evaporation of water. For this, an original model based on differential mass and energy balances was developed. Two limiting cases were considered. Case 1 was isolated system with an initial oxygen concentration of air while the second case was an isolated system with an endless depot of oxygen. The simulations were done in *MATLAB version 2018a* using standard ode solvers. This master thesis was done at KTH and *Stockholm Exergi* in cooperation *SLU*.

1.2 Specific research questions

The project addressed three specific research questions.

- How to model degradation caused by biological, chemical and physical processes?

- How do the different processes interact with each other, and which ones are the most crucial in controlling material loss?

- Can the model predict thermal runaway?

1.3 Method & methodology

The process of biomass degradation is slow. A theoretical study is therefore suited to investigate the problem. The created model involves biochemical, chemical and physical processes. The individual components were theoretically and numerically investigated individually before all elements were combined. A uniform small volume element have been considered. This volume element have been exposed to different conditions to simulate different cases. The model was compared to data from field studies in order to show its validity and understand its limitations.

1.4 Delimitations

This project was delimited to 20 weeks. There are several types of biomasses that may be used in industrial processes which all have unique physical properties. Stockholm Exergi uses forests logging residues in their boilers. Norway spruce is largely present in forest residues from Nordic countries and this work has therefore been delimited to Norway spruce as the principle biomass. [1] Data from field studies have been taken from Nykvarn, Sweden. The field study were conducted between February to August in 2017 by Erik Anerud, who kindly provided the raw data which is included in this project.

Chapter 2 - Background

2.1 Storage of biomass

2.1.1 Overview

EU targets reduced greenhouse gas emissions by 40% compared to 1990 by 2030. An increased utilization of renewable energy sources such as biomass needs to be applied to reach the global energy and environmental goals set for the coming future. [2] Biomass may be used for conventional combustion in combined heat and power plants, which is the case at Stockholm Exergi. The effective heating value of biomass varies but can be around 20 MJ/kg dry basis. [3] An important industrial process for biomass is biomass gasification. Biomass gasification produces products which can be used in various applications such as heat and power production. The gasification process is a thermochemical process that generally involves the following steps: drying, pyrolysis, partial combustion and gasification. Pyrolysis is the process of thermally decompose carbonaceous biomass under anaerobic conditions. Common products from pyrolysis are charcoal, oils and syngas. [4] Biomass is usually harvest at specific times of the year and often contains a high moisture level after harvest. A high water content lowers the net calorific value since a lot of energy is spent to evaporate water. [5] It is necessary to have large scale storage facilities for biomass for two major reasons. These reasons are to let the material dry and to match periods of high demands. Biomass comes in a variety of forms and from a varietry of places. Forest residuals also known as GROT is often used in Sweden. The moisture content in fresh forest residues is usually around 40-55 wt% dry basis. [6] Material degradation and heat generation are commonly observed in stored stacks of chipped wood. [7]

Forest residuals are made up by a matrix of materials such as bark, needles, sapwood, heartwood and inorganic matter. The ratio of these materials depends on the harvest site. The three major components of wood are cellulose, hemicellulose and lignin. There is also a small portion of smaller sugar units present in fresh GROT. The low mass to volume ratio of forest residuals makes transporting and storing relatively costly and it is thus important to understand the storage behaviour to optimize storage conditions. Forest residuals are chipped in order to compress the material for storage and transport. Uncominuted GROT typically cannot be transported for longer distances than 40 kilometers if it is to be economicaly viable. Chipped GROT can be transported for longer distances but chipping also increases the risk of energy losses during storage. Energy losses occur both due to quality degradation and the direct loss of material itself. [6] Material loss is caused by vaporization of water, living cell respiration, biological degradation and chemical oxidation reactions. [3] The dry matter composition, ash content and moisture content all affect the heating value and thereby fuel prices. [5] Biomass storage can be designed in a variety of ways with ranging costs. Uncovered open air storage is the cheapest option but generally has the highest material loss and quality degradation, while covered storage with climate control costs most but tends to retain higher quality and gives rise to less material loss than other alternatives. Which storage system to chose consequently depends on a lot of parameters such as type of biomass to be stored, geometry and storage time, quantity to be stored, precipitation, wind, transportation distance, end usage etc. [7]

Many studies uses net-bags to measure dry matter (DM) losses. These bags are filled with wood substrate and distributed inside the biomass pile. The moisture content and weight is measured and compared before and after storage. Hofman et al. performed field experiments in south Germany in 2018. Here, spruce wood chips were stored between November of 2014 to 2015 of April as well as between May to October in 2015. Two piles of around 200 m^3 were built in each storage period. One pile was covered with nonwoven polypropylene fleece while the other pile was kept uncovered. Degradation measurements were done by placing 144 balance bags inside each pile. After five months of summer storage, 11.1 % had degraded in the covered pile while 7% DM degraded in the uncovered pile. In the winter, 8% was degraded in the covered pile while 7.8% was degraded in the uncovered pile. [8]

Another problem in biomass storage is the self-heating that goes along with the previously mentioned mechanisms that causes material loss. Microbial activity, chemical oxidation reactions and adsorption of water produces heat. The heat transfer inside and from a biomass stack is limited which causes a rise in temperature. [3] The self-heating process may lead to self-ignition which can lead to fires. There have been multiple reports of self-ignited fires. For example in Arlöv, Sweden a pile of wood chips caught fire in 2011. [9]

One solution to reduce DM losses during storage and terminate the risk of self-ignition could be to add chemical additives which reduces microbial activity into the storage pile. A study on chemical additives was performed in 1973 by Wallace E. Eslyn. Thirty different addiatives were investigated with incubation tests on red pine. Several chemicals were evaluated as successive in reducing microbial activity. However, the additives effect on the thermal oxidation reaction in the boiler also have to be considered. Most of the investigated chemical substances would result in undesired oxidation reactions. [10]

2.1.2 Degradation mechanisms

Living cell respiration

Living cell respiration is the name of the automotive catabolic process that converts glucose into ATP in plants. This reaction involves several steps but the net heat released from the overall process is 1100 kJ/mol. Temperatures around 60°C terminates the reaction by inactivating enzymes involved in cell respiration. This process is short lived in chipped piles, where it can prolong between 10 and 40 days. [3]

Biological degradation

There are various microorganisms and bacteria that can degenerate wood. However, the mobility of bacteria is limited to transport in liquid water since they expand by cell division. The degradation by bacteria is therefore less of a problem than degradation by other wood-decaying organisms. The biological degradation of wood is caused by enzymes introduced by wood consuming organisms. The enzymes transform insoluble molecules to soluble chemical substances that are used in the metabolism in these organisms. There are a few well known families of fungus that may colonize wood, two of these are Brown-rot and White-rot fungi. Brown-rot usually prefers soft-wood while White-rot usually prefers hard-wood. Brown-rot mostly degrade polysaccharides but they also break down lignin to a lesser degree. White-rot fungi degrades all of the major components of wood but has a preference to lignin. [11] A portion of degraded substrate is used to grow new fungi while the rest is used in metabolism. [12]

The biological degradation rate caused by microorganism is dependent on the present moisture and oxygen content as well as on the temperature. Different microorganisms operate during different temperature windows. The activity of wood-decaying microorganisms is terminated around 60-65°C. [3] Yu Fakasawa investigated the growth rate of Brown-rot and White-rot fungi species in Pinus densiflora deadwood in the temperature span of 5-40°C. It was concluded that Brown-rot fungi have optimum growth rates at around 30°C while White fungus show optimum rates between 20-30°C. [13] Almost all microbial activity only occurs if the water content is above the fiber saturation point (around 20-25 wt%) as fungi require water to grow. If the moisture content gets to high the degradation slows down since the oxygen solubility in water is quite low. Measuring the effect of moisture is hard since moisture gradients exists within the wood and since it is difficult to keep the water content constant over long periods. [14] Microbial activity occurs in both aerobic and anaerobic conditions. Aerobic degradation goes faster and causes emissions of carbon dioxide and carbon monoxide. [3] Methane, alcohols and organic acids are produced in anaerobic conditions. [15] The heat production is less under anaerobic conditions. [16]

In 2011, Ferrero et al. published results from temperature and gas measurements from various positions inside a heap of pine wood, the dimensions of the stack were $20 \times 15 \times 6$ m^3. Their experiments showed a steep increase in temperature inside the heap within the first 10-20 days. The authors suggested that the fast initial increase in temperature is caused by consumption of free sugar species that become largely

available after chipping. The free sugars can be consumed by a larger population of microbial species than the cellulose, hemicellulose and lignin. This would result in a decrease in heat generation once the easily degradable portion is consumed. Furthermore, emissions of methane was recorded on up to 60 ppmv, indicating very little fermentation inside the stack. The inner temperature in the stack decreased when the other layer froze. An explanation could be that the oxygen diffusion into the pile was hindered which caused a decrease in microbial activity. [17] Whittaker et al. did a similiar study. Measurements of methane emissions reached a peak around 400 ppmv after 40 days. This occurred after the first spike of carbon dioxide, indicating anaerobic conditions inside the pile. All measured emissions reached a baseline after 60 days, the carbon dioxide emission were below 5000 ppmv while the methane production were below 50 ppmv. [18]

Thermal degradation and chemical oxidation reactions

Chemical oxidation of wood is slow at moderate temperatures and is therefore not the initial driving force in material loss and heat generation in large-scale wood chip storage. [3] When the heat production surpasses the heat dissipation the reaction will accelerate and eventually result in self-ignition and massive material loss. Multiple products are produced when wood undergoes thermal degradation. The thermal degradation process depends on atmosphere, pressure, temperature, heating rate, time of exposure and moisture content. [11], [4] Examples of products from thermal degradation are char, tar, volatile liquids, carbon monoxide, carbon dioxide, methane, hydrogen and water. Char is a carbon residue. [19]. Thermal analysis of biomass is generally carried out by thermal gravimetric analysis (TGA) and differential scanning calorimetry (DSC) at high temperatures. Generally, a TGA scheme of wood shows an endothermic peak around 100°C which is the result of evaporation of water. This peak is followed by exothermic degradation processes at elevated temperatures. The exothermal peaks are observed in higher temperature intervals during oxygen free analysis. Maryandyshev et al. analyzed spruce with a gas flow rate of $20 \cdot 10^{-5}$ m^3/min of either air or argon, and a heating rate of 10 °C/min. The suggested scheme from this article included three steps: drying, devolatilization and char combustion. Emissions of volatile compounds occur in the devolatilization phase. Drying ended at 92°C in air and at 120°C in argon. The devolatilization proceeded between 210-340°C in air while between 221-377°C in argon. The char was combusted in air between 347-503°C. A lower calorific value of 18.7 MJ/kg for spruce was determined through DSC. [20] Chemical bonds in wood start to break above 100°C. The thermal degradation between 100-200°C produces water vapour, non combustible gases and liquids, such as carbon monoxide, carbon dioxide, some acids and volatile organic compounds. The thermal degradation of cellulose, hemi cellulose and lignin is slow in this temperature interval. However, the auto-oxidation rate increases. Oxidation is the result of air diffusing and reacting with char. [21] The effects of prolonged heat exposure of spruce wood was measured by Fengel in 1966. The temperatures was raised and kept constant for 24 hours in the interval of 100-200°C. Weight losses in the magnitude of 0.8 wt% began at 120°C. The weight loss reached 15.5 wt% at 200°C. [11]

Physical transformation of water

The moisture content of wood has several implications on the degradation outcome and heat generation. As discussed above, fungi and bacteria need moisture to degrade wood but there are also a direct connections to heat production/consumption related to the physical transformation of water. Condensation releases heat while evaporation is an endothermic process. [3] Furthermore, the heating value of water is more than two times higher than that of dry wood. It therefore takes substantially more energy to cause the same rise in temperature in heavily wet wood than in dry wood. [22]

Chapter 3 - Modeling

This chapter presents the model developed and tested in this project. Some parameters are explained in the text, see the nomenclature list for the rest. The chapter starts by going through each sub-model before combining these processes and investigating different cases and comparing them to raw data.

3.1 Microbial activity

Microbial degradation of forest residuals (substrate) is an important aspect to consider since it is the initial cause of heat generation and dry matter loss for modeling microbial activity. The substrate was divided into three fractions. One of these fractions is hard to degrade and hence degrades slowly (S_H). One fraction is easy to degrade, this fraction degrades fast in relation to the slow fraction (S_E). The third fraction is inert and does not degrade at all (S_I). The hard to degrade fraction is composed of cellulose, lignin and hemicellulose while the easily degradable fraction consists of extractives such as smaller sugar units. The inert fraction is composed of inorganic material. The biological degradation sub model was based on the assumptions listed below. These assumptions are based on the information gathered and displayed in the background section of the report.

- Forest residuals of Norway spruce consists of 90% slowly degradable macro molecules, 8% of easily degradable extractives and 2% of inert inorganic material (dry basis).

- The intial moisture content is 55 wt% (dry basis).

- The extractives are modeld as $C_6H_{12}O_6$

- Starting at 15°C, within a week, the bulk density of extractives are consumed and a considerable amount of wood decaying microorganisms has been formed. The degradation rate slows down but material keeps degrading if oxygen is supplied and temperature is controlled. Having optimal temperature, oxygen and moisture for degradation, a magnitude of around 50% is expected to have degraded within six months. This degradation percentage is in the magnitude suggested by Erntson et al. [15], [22]

- Heat generation is significant in the initial week, and then slows down just as the material degradation. The heat generation leads to an increase in temperature. Microbial degradation stops at 65°C.

- Heat generations is related to oxygen consumption and carbon dioxide production. Heat generation is modeled as aerobic respiration:

$$C_6H_{12}O_6 + 6\ O_2 \rightarrow 6\ CO_2 + 6\ H_2O_{(l)}$$

$$\Delta H_R = -1100 \left[\frac{kJ}{mol\ CO_2} \right]$$
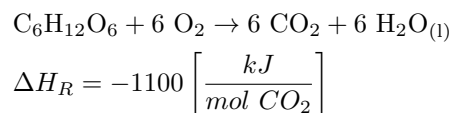
- Microorganism colonization and growth can only occur at water contents over 25 wt% (dry basis). Higher moisture contents does not affect the degradation rate.

- The degradation rate is proportional to oxygen concentration.

- The degradation rate is slow at temperatures below 15°C and then rapidly increases. It is highest in the temperature range of 20-30°C. The rate rapidly decreases at temperatures above 50°C.

The reaction pathway was based on the work of Ferrero et al. The macro-molecules that are hard to degrade is hydrolyzed into extractives (reaction r_1 in figure 3.1). These extractives can both be metabolized by wood-decaying organisms and used to grow new cells (reaction r_2 in figure 3.1). The portion of the degraded

substrate that is used for metabolism gives rise to carbon dioxide, liquid water and heat. The microorganisms also dies with time (reaction r_3 in figure 3.1). This pathway is depicted in figure 3.1 [23]
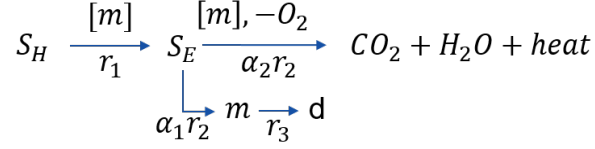
$$S_H \xrightarrow[r_1]{[m]} S_E \xrightarrow[\alpha_2 r_2]{[m], -O_2} CO_2 + H_2O + heat$$
$$\alpha_1 r_2 \searrow m \xrightarrow{r_3} d$$

Figure 3.1: The bio-activity sub-model has been based on the following reaction scheme.

Assuming a closed system uniform in space, the reaction scheme above is translated into the following system of equations:

$$\dot{\rho}_{S_H} = -r_1 \tag{3.1}$$

$$\dot{\rho}_{S_E} = r_1 - r_2 \tag{3.2}$$

$$\dot{\rho}_m = \alpha_1 r_2 - r_3 \tag{3.3}$$

$$\dot{\rho}_d = r_3 \tag{3.4}$$

$$\dot{\rho}_{O_2} = -6\alpha_2 \frac{M_{O_2}}{M_{S_E}} r_2 \tag{3.5}$$

$$\dot{\rho}_{CO_2} = 6\alpha_2 \frac{M_{CO_2}}{M_{S_E}} r_2 \tag{3.6}$$

$$\dot{\rho}_{(W,L)} = 6\alpha_2 \frac{M_{H_2O}}{M_{S_E}} r_2 \tag{3.7}$$

Here, $\dot{\rho}_i$ is the time derivative of the density for specie i, r_j denotes the reaction rate of reaction j, M_i is the molar mass of component i and α_k expresses the mass-based stoichumetric coefficient of reaction r_2, obeying $\alpha_1 + \alpha_2 = 1$. The reaction rate expressions are similar to those proposed by Michaelis-Menten for enzymic reactions.

$$r_1 = -\frac{k_1 \rho_{S_H}}{K_{S_1} \rho_m + \rho_{S_H}} \rho_m g_1(T) g_2(O_2) g_3(H_2O) \tag{3.8}$$

$$r_2 = \frac{k_2 \rho_{S_E}}{K_{S_2} + \rho_{S_E}} \rho_m g_1(T) g_2(O_2) g_3(H_2O) \tag{3.9}$$

$$r_3 = k_3 \rho_m g_1(T) g_2(O_2) g_3(H_2O) \tag{3.10}$$

More specifically, these reactions rates are Monod-kinetic rate expressions which are empirical expressions commonly used in the field of biological degradation. [23] The rate expressions are further dependent on temperature, oxygen and moisture. These dependencies are modeled with the functions g_i. The temperature and oxygen dependence was modeled in a similar way to what was described by Ernstson et al. The dependency functions are all bounded in the interval of $[0, 1]$. [22]

Table 3.1: Values used when simulating micro-activity. [23]

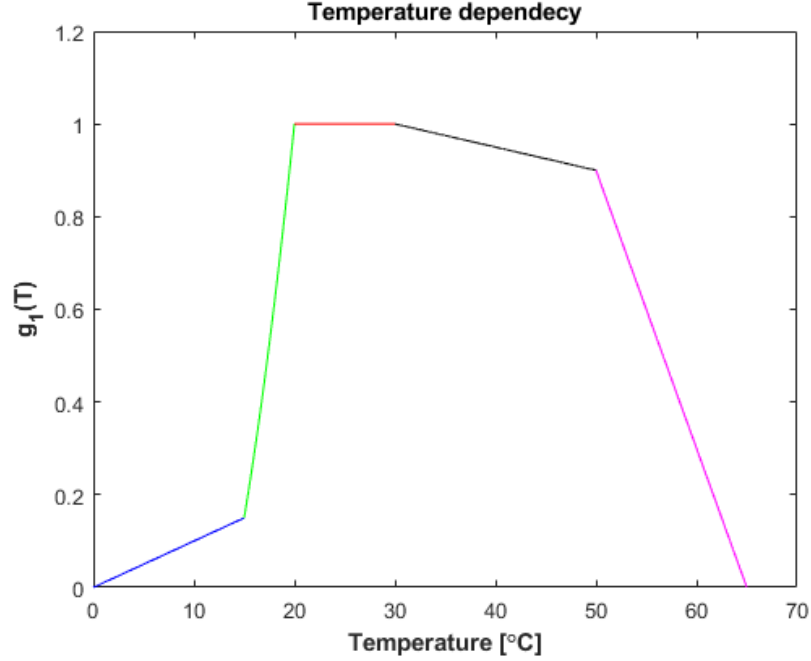| $k_1 \ [s^{-1}]$	$k_2 \ [s^{-1}]$	$k_3 \ [s^{-1}]$	K_{S_1}	$K_{S_2} \ \left[\frac{kg}{m^3}\right]$	$\rho_{m0} \ \left[\frac{kg}{m^3}\right]$	$\Delta H_R \ \left[\frac{kJ}{kg}\right]$ [3]	α_1	α_2
$4.244 \cdot 10^{-5}$	$7.094 \cdot 10^{-5}$	$2.755 \cdot 10^{-5}$	52	$9.317 \cdot 10^{-3}$	$3.45 \cdot 10^{-2}$	-25000	0.68	0.32

Figure 3.2: The temperature dependency have been modeled with different functions for different intervals shown with the different colors.

- The temperature dependence was modeled as the piece-wise linear function, depicted in figure 3.2.

- The oxygen dependence was modeled as the following linear function:

$$g_2(O_2) = \frac{p_{O_2}}{p_{O_{2,air}}} \tag{3.11}$$

Where p_{O_2} is the actual partial pressure of oxygen and $p_{O_{2,air}}$ is the partial pressure of oxygen in air.

- The moisture dependence was modeled as a step function.

$$g_3(H_2O) = 1, \ \omega_{(W,L)} \geq 25 \ wt\% \\ 0, \ \omega_{(W,L)} < 25 \ wt\% \tag{3.12}$$

It is assumed that only processes that produce carbon dioxide and water contribute to heat generation. Accordingly, the heat generation reads as:

$$\dot{S}_{T_B} = 6\alpha_2 \frac{M_{CO_2}}{M_{S_E}} \Delta H_R r_2 \tag{3.13}$$

Here, $\dot{S}_{T_B}$ is the heat source expressed in kJ/(m³ · s). The factor 6 comes from the stoichiometry of the reaction.

From the mechanism shown in figure 3.1 it can bee seen that all bio-degradation stops if the microorganisms dies since they catalyzes both pathways of degradation. However, in reality the microorganisms will not die if the conditions in the pile are favorable. A stability and dynamic analysis of this sub-model was performed to investigate how the concentration of microorganisms evolves with time. Parameter values used when simulating degradation are shown in table 3.1. Most values were taken from the research presented

by Ferrero et al. [23] The value of K_{S_1} was adjusted to match the degradation pattern described in the assumptions. This parameter was altered as a response to the analyses previously described. A conclusion from the stability analysis were that two conditions must be satisfied to keep the microorganisms alive:

$$\alpha_1 k_2 > k_3, \ \alpha_1 k_1 > k_3 \tag{3.14}$$

These conditions are met for the parameter values listed in table 3.1. See appendix A for additional information about how this system was derived.

3.2   Chemical oxidation

Chemical oxidation is the cause of material loss at elevated temperatures, in which the microorganism die and microbial activity stops. The chemical oxidation of wood is a complex phenomena at temperatures above 200°C. A lot of the mechanism is yet to be understood. However, the model will focus on a lower temperature interval since massive losses occur at temperatures above 200°C. The model aims to predict how to avoid getting such high temperatures in the pile. The chemical oxidation reaction was simplified to complete combustion. This case generates most low energy density gaseous products which hinders transport while generating the maximum amount of heat leading to maximum heat accumulation and threats of runaway phenomena. It can therefore be consider to be the worst case. The chemical oxidation sub model was based on the assumptions listed below. These assumptions are based on information presented in the introduction.

- The chemical oxidation is negligible at low temperatures and slow between 80-100°C. Prolonged exposure at 120°C results in degradation.

- The weight loss during the first 24 hours is very low at a constant temperatures of 120°C.

- The weight loss during the first 24 hours reaches a magnitude of 15-20 wt% at a constant temperature of 200°C.

- The oxidation products are carbon dioxide and water.

- The substrate degradation is of first order with respect to the substrate.

- The reaction rate depends on the temperature and the partial pressure of oxygen.

- The heat production is modeled with the lower calorific value of 18.7 [MJ/kg].

Table 3.2: Parameters used to simulate chemical oxidation.

| ν_1	ν_2	ν_3	k_0 $[s^{-1}]$ [23]	E_A/R $[K]$ [23]	ΔH_C $\left[\frac{MJ}{kg}\right]$ [20]
1.0565	1	0.67795	$8.15 \cdot 10^5$	$12,509$	-18.7

The substrate composition has been decided based on the chemical composition data for GROT presented in *Bränslehandboken 2012* . The composition on moisture and ash free basis is 53.1 wt% C, 6 wt% H, 40 wt% O, 0.04 wt% S, 0.31 wt% N and 0.02 wt% Cl. [6] Weight fractions is converted to molar fractions by equation 3.15.

$$x_i = \frac{\frac{\omega_i}{M_i}}{\sum \frac{\omega_j}{M_j}} \tag{3.15}$$

Ignoring S, N and Cl, the composition on the normalized form thus reads as:

$$C_1 H_Y O_Z$$
$$Y = 1.3559 \tag{3.16}$$
$$Z = 0.5650$$

The following reaction pathway have been used to simulate oxidation.

$$C_1 H_Y O_Z + \nu_1\ O_2 \rightarrow \nu_2\ CO_2 + \nu_3\ H_2O \tag{3.17}$$
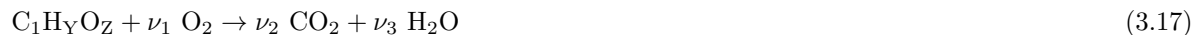
The density source terms and heat generation was modeled as a first order kinetic reaction with respect to the substrate. This approach have been applied in many studies. [24], [23], [25] The degradation is also proportional to the oxygen concentration.

$$\dot{\rho}_S = r_4 = -(\rho_{S_H} + \rho_{S_E})k_0 e^{(-E_A/(RT))} g_2(O_2) \tag{3.18}$$

Where k_0 is the pre-exponential factor, E_A is the activation energy, R is the gas constant, the oxygen dependency is shown in equation 3.11.

Assuming a spatially uniformed closed system, the following equations describes degradation and heat generated by chemical oxidation.

$$\dot{\rho}_{S_H} = -\frac{\rho_{S_H}}{\rho_{S_H} + \rho_{S_E}} r_4 \tag{3.19}$$

$$\dot{\rho}_{S_E} = -\frac{\rho_{S_E}}{\rho_{S_H} + \rho_{S_E}} r_4 \tag{3.20}$$

$$\dot{\rho}_j = -\nu_j \frac{M_j}{M_S} r_4 \tag{3.21}$$

$$\dot{S}_{T_C} = \Delta H_C r_4 \tag{3.22}$$

Here, $\dot{S}_{T_C}$ is the heat source expressed in kJ/(m³ · s), ΔH_C is the heat of combustion and ν_j denotes the stoichiometric coefficient of substance j. Stoichiometric coefficients are negative for reactants and positive for product species. See appendix B for additional information for how the system was derived.

3.3   Physical transformation

Condensation and evaporation of water was treated by considering saturated atmosphere with respect to water vapor inside the porous media. The pressure/density of water vapor then becomes a function of temperature. The change in water vapor therefore has to be coupled with the temperature evolution with time which is gained from the energy balance of the system. This is shown below in equation 3.23. The assumption that the system is saturated provides a convenent modelling framework that also was adopted in earlier works [15]. See appendix C for an evaluation of the physical transformation sub-model.

$$\dot{\rho}_{(W,V)} = \frac{dT}{dt} \frac{d\rho_{(W,V)}}{dT} \tag{3.23}$$

The vapor pressure may be related to the temperature inside the stack through an emperical expression called Antoine's law.

$$\log p_{(W,V)} = A - \frac{B}{T + C} \tag{3.24}$$

Here, A, B and C are substance specific constants expressed. Combining Antoine's law with the ideal gas law allows the density to be expressed as a function of temperature.

$$\rho_{W,V}(T) = \exp\left(A - \frac{B}{T + C}\right) \frac{M_{H_2O}}{RT} f\epsilon \tag{3.25}$$

Where f is a conversion factor and ϵ expresses the porosity of the bed. The temperature derivative of equation 3.25 is given below:

$$\frac{d\rho_{(W,V)}}{dT} = f\epsilon \frac{M_v}{RT} \exp\left(A - \frac{B}{T + C}\right) \left(\frac{B}{(C + T)^2} - \frac{1}{T}\right) \tag{3.26}$$

Parameter values used in equation 3.26 are listed in table 3.3

Table 3.3: Parameter values used to describe physical transformation. Antoine's constants are adjusted for natural logarithm and Kelvin.

A [26]	B [26]	C [26]	ϵ	$f \left[\frac{kgPa}{gmmHg}\right]$
18.669	403.02	-38.15	0.5	$10^{-3} \cdot 133.32$

3.4 Transport

Transport of species may be caused by different phenomena such at diffusion, natural convection, buoyancy forces or external flows. Wind could be modeled as an external flow in which addition of oxygen and nitrogen into the pile is added. Diffusion is caused by random motions of molecules and is expressed by fick's law, see equation 3.27. [27]

$$N_{A_1} = -D_A \nabla C_A \quad \left[\frac{kg}{m^2 s} \right] \tag{3.27}$$

Transport caused by natural convection and buoyancy forces in a pile is an effect of the temperature increase inside the stack. The increasing temperature leads to an increase in pressure which creates natural convection. Natural convection caused by a pressure increase in porous media is controlled by Darcy's Law, which is shown below in spacial direction i for a laminar flow. [28]

$$N_{A_2} = -\rho_A \frac{\beta}{\mu l_i} \Delta p \quad \left[\frac{m}{s} \right] \tag{3.28}$$

Buoyancy forces act on densities which becomes lower at elevated temperatures. This means that a coherent movement of gaseous species in an upwards direction within the pile is initiated. The hot gases are replaced by colder gases. Buoyancy effects are expressed equation 3.29. [29]

$$N_{A_3} = g \Delta \rho_A \left[\frac{kg}{m^2 s} \right] \tag{3.29}$$

Ferrero et al. considered transport by diffusion and convection. Convection was considered by increasing diffusion coefficients. Diffusion is caused by random movements of molecules, here the flux is driven by a concentration gradient. [23] Ernstson et al. investigated the importance of convection by studying the Rayleigh number. The Rayleigh number can be expressed on an energy basis as well as on a mass basis. This number shows the ratio of heat transferred by free convection and conduction or the ratio of mass transferred by natural convection and diffusivity. Ernstson et al. concluded that natural convection is important when describing transfer in a wood pile. [22]

The interplay between these transport mechanisms needs further investigations through literature before being implemented into the model. In the following section energy and mass balances have been setup for a small homogeneous volume element. These balances include a transport term but only isolated cases were performed to evaluate the model. The following section develops this modelling approach further.

3.5 All processes

All processes were lastly combined and examined together to get an understanding for how these processes interact with each other. Consider the volume element shown in figure 3.3. If a small volume is consider the system can be treated as homogeneous. Conditions may then be changed to consider different placements inside the pile.

3.6 The general case

The mass balances over the system are described below, these are mostly based on the sub-models which are previously described in the report. An additional transport term was added to these balances. The mass balances includes biochemical reactions (green), chemical oxidation reactions (red), physical transformation of water (blue) as well as transport (black).

$$\dot{\rho}_{S_H} = -r_1 - \frac{\rho_{S_H}}{\rho_{S_H} + \rho_{S_E}} r_4 \tag{3.30}$$

$$\dot{\rho}_{S_E} = r_1 - r_2 - \frac{\rho_{S_E}}{\rho_{S_H} + \rho_{S_E}} r_4 \tag{3.31}$$

$$\dot{\rho}_{S_I} = 0 \tag{3.32}$$

$$\dot{\rho}_m = \alpha_1 r_2 - r_3 \tag{3.33}$$

$$\dot{\rho}_d = r_3 \tag{3.34}$$

$$\dot{\rho}_{(W,V)} = \frac{dT}{dt} f \epsilon \frac{M_v}{RT} \exp\left(A - \frac{B}{T+C}\right) \left(\frac{B}{(C+T)^2} - \frac{1}{T}\right) \tag{3.35}$$

$$\dot{\rho}_{O_2} = -6\alpha_2 \frac{M_{O_2}}{M_{S_E}} r_2 - \nu_1 \frac{M_{O_2}}{M_S} r_4 - \frac{F_{O_2}}{V} \tag{3.36}$$

$$\dot{\rho}_{CO_2} = 6\alpha_2 \frac{M_{CO_2}}{M_{S_E}} r_2 + \nu_2 \frac{M_{CO_2}}{M_S} r_4 - \frac{F_{CO_2}}{V} \tag{3.37}$$

$$\dot{\rho}_{(W,L)} = -\dot{\rho}_{(W,V)} + 6\alpha_2 \frac{M_{H_2O}}{M_{S_E}} r_2 + \nu_3 \frac{M_{H_2O}}{M_S} r_4 - \frac{F_{W,V}}{V} \tag{3.38}$$

$$\dot{\rho}_{N_2} = -\frac{F_{N_2}}{V} \tag{3.39}$$

The energy balance that describes the temperature evolution is shown in equation 3.40.

$$\dot{T} = \frac{Q - \frac{F_{(W,V)}}{V}\Delta H_{Vap} - 6\alpha_2 \frac{M_{CO_2}}{M_{S_E}}\Delta H_R r_2 - \Delta H_C r_4}{\sum \rho_i c_{p,i} + \frac{d\rho_{(W,V)}}{dT}\Delta H_{Vap}} \tag{3.40}$$

Where, Q represents the heat transfer with the surroundings, $-\frac{F_{(W,V)}}{V}\Delta H_{Vap}$ is the heat that leaves the system through water transport, $-6\alpha_2 \frac{M_{CO_2}}{M_{S_E}}\Delta H_R r_2$ and $-\Delta H_C r_4$ are the heat generating terms from the bio chemical and chemical reactions, respectively. The denominator shows that heat are used to heat up the system as well as to evaporate water. It is important to note that the specific heat capacity of the substrate depends on its moisture level. This relationship is expressed in equation 3.41.

$$c_{p,s} = \frac{c_{p,(W,L)}\omega_{(W,L)} + c_{p,DM}}{\omega_{(W,L)} + 1} \tag{3.41}$$

Initial conditions

The initial concentrations of gaseous species are dependent on the initial temperature and pressure of the system. The pressure is initially built up by water vapor, oxygen and nitrogen. The numbers presented here corresponds to an initial pressure of 1 atm and a starting temperature of 15°C. The atmosphere is saturated with water vapor. The solid is assumed to be porous material with an apparent density of 410 kg/m³, comprised of 90 wt% hard to degrade substrate, 8 wt% easy to degrade substrate and 2 wt% inert inorganic material. All concentrations have the unit kg/m³.

$$\begin{aligned}
&\textit{Gaseous species}: \rho_{(W,V)_0} = 0.0064, \ \rho_{O_{2_0}} = 0.1397, \ \rho_{CO_{2_0}} = 0, \ \rho_{N_{2_0}} = 0.4598, \\
&\textit{Liquid species}: \rho_{(W,L)_0} = 225.5, \\
&\textit{Solid species}: \rho_{S_{H_0}} = 369, \ \rho_{S_{E_0}} = 32.8, \ \rho_{S_{I_0}} = 8.2, \ \rho_{m_0} = 3.45 \cdot 10^{-2}, \ \rho_{d_0} = 0
\end{aligned} \tag{3.42}$$

Cases

Two cases were run to evaluate the model. The first case looks at an insulated system, meaning that no heat or mass is exchanged with its surroundings. Here the initial oxygen concentration is equal to that in air. The second case is an insulated system with an endless depot of oxygen. The two cases were run to see how the system behaves at these two extremes. These two cases are purely theoretical and are only set up to investigate the model. The second case could be consider a worst case scenario since all heat is accumulated within the system, while the unlimited supply of oxygen keeps the degradation processes going.

The system – the control volume

Volume: $\sim 10^{-2}$ [m]

Bio-chemical reactions
Chemical oxidation reactions
Evaporation/condensation of water

$F = F_{out} - F_{in} \left[\dfrac{kg}{s} \right]$

$Q \left[\dfrac{kJ}{m^3 s} \right]$

Black – inflow (mass)
Pink – outflow (mass)
Purple – heat flow
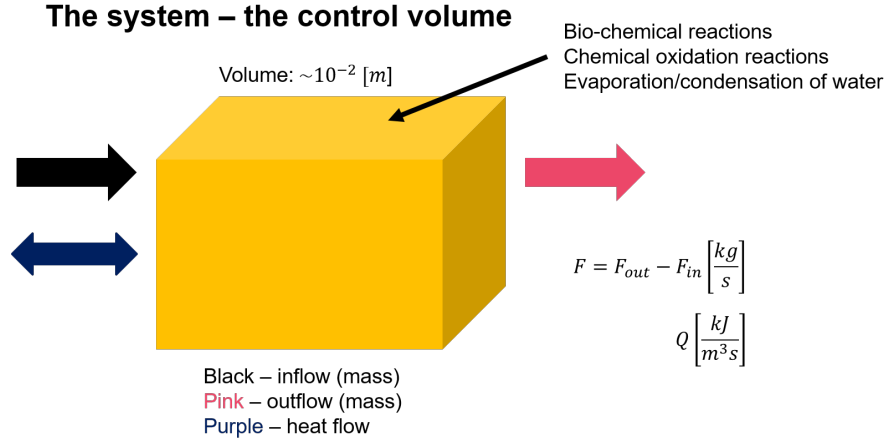
Figure 3.3: The system is a homogeneous volume element.

3.6.1   Case 1 - 'Deep inside the stack' (No boundary effects)

The system becomes a insulated system if no boundary effects are considered since all neighbouring elements have the same temperature and pressure evolution, eliminating all driving forces for transport. The mass and energy balances were therefore transferred into the system presented here.

$$\dot{\rho}_{S_H} = -r_1 - \frac{\rho_{S_H}}{\rho_{S_H} + \rho_{S_E}} r_4 \tag{3.43}$$

$$\dot{\rho}_{S_E} = r_1 - r_2 - \frac{\rho_{S_E}}{\rho_{S_H} + \rho_{S_E}} r_4 \tag{3.44}$$

$$\dot{\rho}_{S_I} = 0 \tag{3.45}$$

$$\dot{\rho}_m = \alpha_1 r_2 - r_3 \tag{3.46}$$

$$\dot{\rho}_d = r_3 \tag{3.47}$$

$$\dot{\rho}_{W,V} = \frac{dT}{dt} f\epsilon \frac{M_v}{RT} \exp\left(A - \frac{B}{T+C}\right)\left(\frac{B}{(C+T)^2} - \frac{1}{T}\right) \tag{3.48}$$

$$\dot{\rho}_{O_2} = -6\alpha_2 \frac{M_{O_2}}{M_{S_E}} r_2 - \nu_1 \frac{M_{O_2}}{M_S} r_4 \tag{3.49}$$

$$\dot{\rho}_{CO_2} = 6\alpha_2 \frac{M_{CO_2}}{M_{S_E}} r_2 + \nu_2 \frac{M_{CO_2}}{M_S} r_4 \tag{3.50}$$

$$\dot{\rho}_{W,L} = -\dot{\rho}_{W,V} + 6\alpha_2 \frac{M_{H_2O}}{M_{S_E}} r_2 + \nu_3 \frac{M_{H_2O}}{M_S} r_4 \tag{3.51}$$

$$\dot{\rho}_{N_2} = 0 \tag{3.52}$$

$$\dot{T} = \frac{-6\alpha_2 \frac{M_{CO_2}}{M_{S_E}} \Delta H_R r_2 - \Delta H_C r_4}{\sum \rho_i c_{p,i} + \frac{d\rho_{W,V}}{dT} \Delta H_{Vap}} \tag{3.53}$$

13

3.6.2 Case 2 - 'Endless depot of oxygen' (Constant optimal oxygen concentration)

This case studies how the model behaves if there is an unlimited amount of oxygen in the insulated system. This yields in the same energy and mass balances as in case 1, although here the function $g_2(O_2)$ is always set to 1 to mimic an unlimited supply of oxygen.

Chapter 4 - Results and discussion

This section presents results from the simulations from case 1 and 2. Five different initial temperatures have been simulated. The five chosen initial temperatures were 5, 10, 15, 20 and 35°C since these temperature starts at different biochemical reaction rates and catches a wide range of possible outdoor temperatures.

4.1   Case 1

The first case looked at an isolated system with an initial oxygen concentration equal to that in air at different initial temperatures. Temperature profiles, oxygen consumption, absolute and percentage based dry matter degradation during and after 60 days of storage are illustrated for this case.

Figure 4.1 shows the temperature profiles for the five different initial temperatures. A slight temperature increase is visible in all cases before the temperature relaxes to a steady-state. Steady-state is reached fastest at an initial temperature of 20°C. At 20°C steady state is reached after approximately 2 days. The transmission towards steady sate is slowest at 5°C where it is reached around 25 days. Steady-state occurs after 5 days of storage at 15°C.

Figure 4.2 shows the oxygen consumption over time in the system. Here it can be seen that the oxygen consumption is slower at lower initial temperatures. The slightly higher initial concentration at lower temperatures are understood after looking at the ideal gas law. The ideal gas law determines that the number of moles increases with decreasing temperatures if the pressure and volume stays constant.

Figure 4.3 shows the absolute substrate degradation of the system. The figure illustrates that only a small amount of the wood degrades by consuming the initial oxygen available in the system. More wood degrades at lower temperatures. The degradation is slower at lower temperatures.

Figure 4.4 shows the degraded percentage after 60 days of storage. A very small amount has degraded. Slightly higher degrdation is seen at lower initial temperatures.

The results from the simulations of the closed system are to be expected. The temperature starts to increase within the first week at an initial temperature of 15°C which is the expected outcome from the micro-activity in the stack. The pattern of increasing time to reach the final temperature state with decreasing initial temperatures below 20°C is caused by slower reaction rates. This also explains why it takes slightly longer to reach the final temperature state when starting at 35°C compared to 20°C. The higher degradation at lower initial temperatures is caused by the increase in initial oxygen concentration. There is more oxygen in the system at lower temperatures. The low total degradation and temperature increase voice that this scenario is far off from the situation occurring in a real biomass stack. However, the importance of including oxygen transport is thoroughly shown by studying this case.
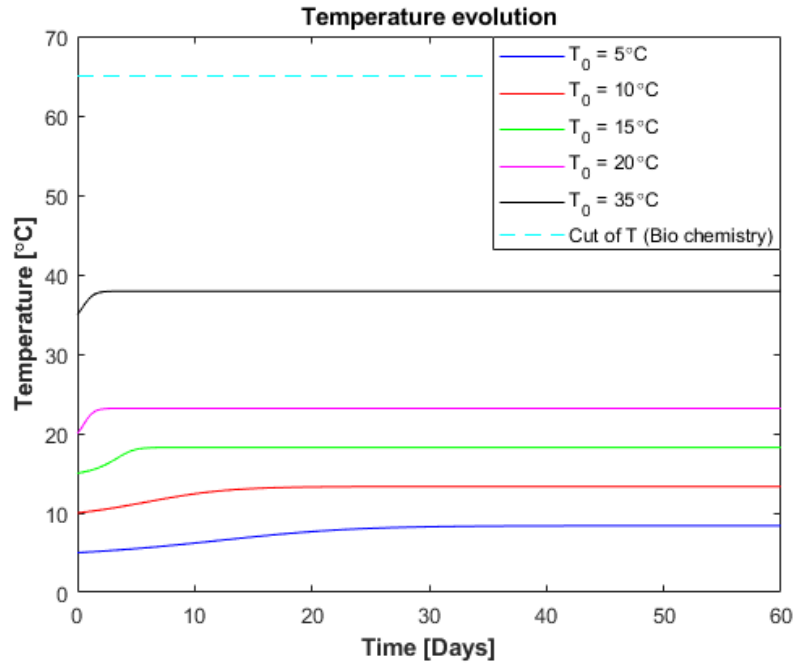
Figure 4.1: Temperature evolution in the isolated system for different initial temperatures. The dashed line shows the critical temperature at which biological activity comes to a rest.
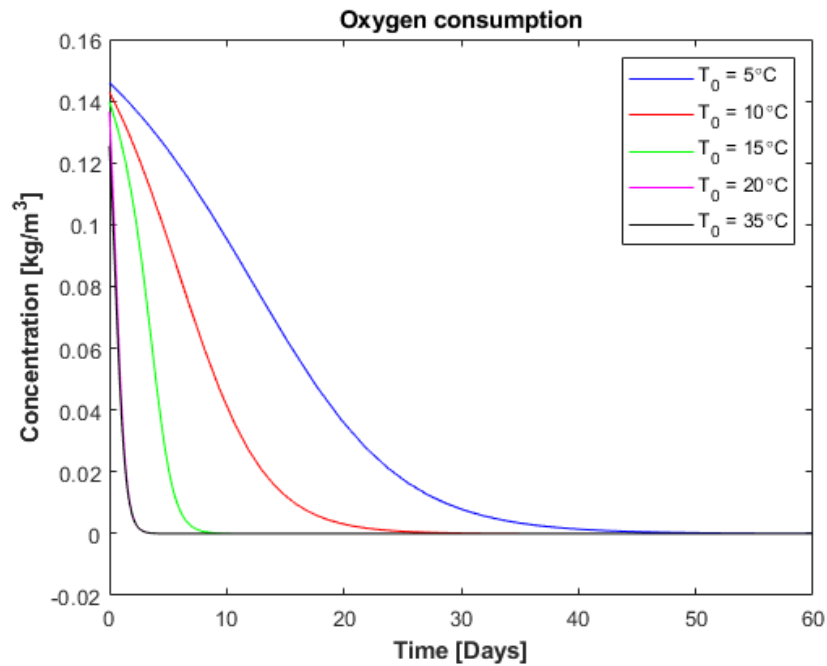

Figure 4.2: Oxygen consumption in the isolated system for different initial temperatures.
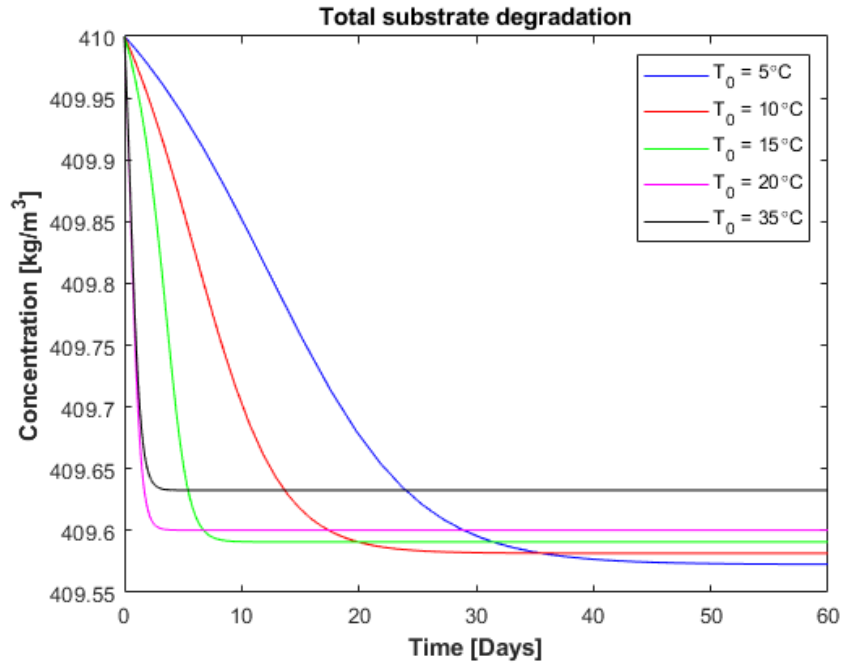
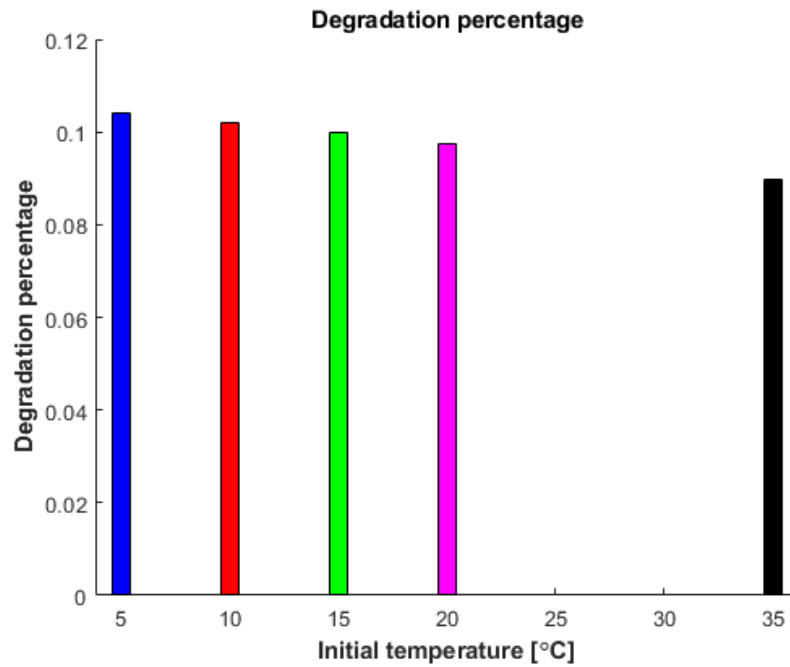Figure 4.3: Substrate degradation in the isolated system for different initial temperatures.

Figure 4.4: Percentage of degradation in the isolated system as a function of the initial temperature.

4.2 Case 2

Case 2 investigated an isolated adiabatic system with an endless depot of oxygen, meaning that the oxygen dependence function $g_2(O_2)$ always equaled 1. Here the temperature evolution, absolute and percentage based degradation are shown for the five initial temperatures. Also displayed here are temperature and humidity evolutions for different initial concentrations of liquid water in the substrate. In these two graphs the initial temperature was set to 15°C. The numerical simulation was stopped at or just before thermal runaway.

Figure 4.5 shows the temperature evolution for the five investigated initial temperatures. The temperature evolves fast until the cut of temperature for microbial activity is reached. Thereafter follows a time of apparent linear evolution which itself is followed by thermal runaway. The apparent linear evolution is expected since the chemical oxidation reaction rate behaves in this manner at constant temperatures.

Figure 4.6 shows temperature profiles for different initial liquid water concentrations at an initial temperature of 15°C. This figure shows that thermal runaway is reached faster for lower initial weight fractions of liquid water. The reason for this is the lower heat capacity of the wet solid matrix.

Figure 4.7 shows the weight fraction of liquid water versus time. The weight fraction of liquid water stays close to constant until thermal runaway is reached. The wood does not dry out in this case before thermal runaway happens since no water is allowed to leave the system. The slight increase is observed since more liquid water is produced in the bio-chemical and chemical reactions than is evaporated to keep the temperature saturated. This stays true until thermal runaway occurs.

Figure 4.8 shows the absolute substrate degradation over time. A fast initial degradation is followed by a period of slower degradation before degradation starts to accelerate again. The fast initial degradation is controlled by microbial activity while the slow degradation in the second stage of the process is controlled by the chemical oxidation reaction.

Figure 4.9 shows the percentage of degraded biomass just before thermal runaway is reached. The degradation percentage varies between 1.5-2.3%. The reason that the degradation is slightly higher for the lower initial temperatures is that the degradation caused by bio-activity proceeds over a larger temperature range.

Figure 4.10 shows how much of the degraded material that was consumed in microbial processes. Here the degradation percentage varies between 0.9 to 1.85%.

Case 2 has optimal conditions for heat accumulation since no heat is transferred to the surroundings while oxygen is always kept at an optimal level for degradation. This case is therefore interesting to look at when investigating how the model predicts thermal runaway. Two important factors to take into account are heat accumulation and how much energy is needed to heat up the system by 1°C. Different weight fractions of water have been looked at to see how long it takes to reach thermal runaway depending on how much liquid water the substrate contains. Starting with a lower initial weight fraction of liquid water than the fiber saturation point (0.25) would prevent microorganism activity which is not interesting to investigate. The fastest thermal runaway occurs after 150 days of storage, which is a much longer time than what is found in the the field study. The model fails to catch the possibility of fast temperature increases all the way up to over 100°C which is observed in some stacks. Some accuracy could be lost due to the fact that the wood is not allowed to get drier after the bio-chemical reaction have reached its cut off temperature. It should however be noted that Stockholm Exergi uses a flue gas condenser which allows the moisture content to be as high as 40%. There is therefore no need to dry the fuel too much before consuming it. The data from the field study also shows a moisture content above 25 wt% at all times. Another important take away from this simulation is that the final degradation percentage from figure 4.9 is around 2.3% while the degradation from the biological processes shown in figure 4.10 are around 1.85%. The degradation is very slow in the temperature range between 65-80°C before chemical oxidation starts to accelerate. The very

slow heat generation in this temperature interval indicates that the model might not predict runaway if heat transfer with the surrounding is added. The temperature range between 65-80°C is therefore considered an area of improvement and need more investigation. This case shows that the microbial processes and chemical oxidation reactions in the model have low interaction with each other. These processes controls material loss in different temperature ranges which is in agreement with literature. However, the gap between these processes must be adjusted to match reality. This case does not reveal the whole truth about how the process of physical transformation interacts with the other processes. To determine this transport of water must be included.
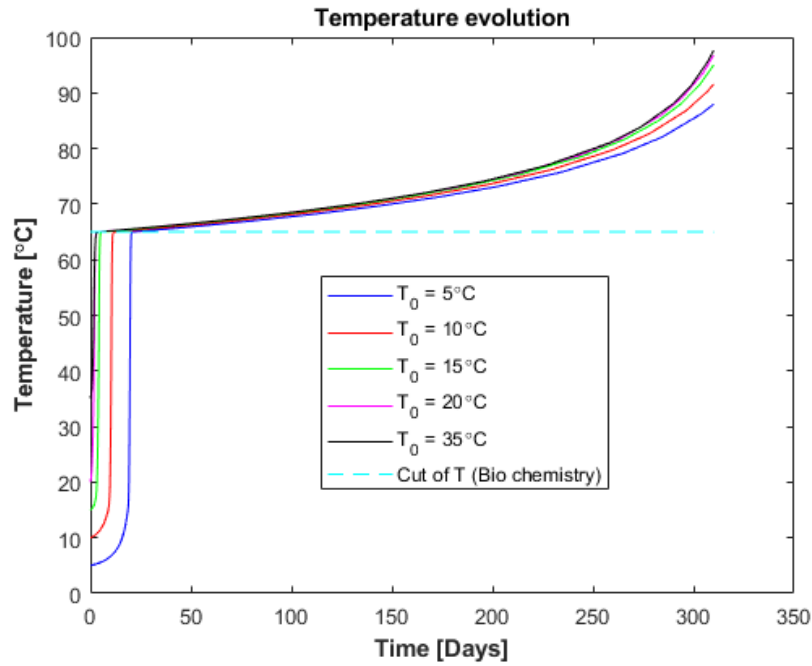
Figure 4.5: Temperature evolution in the adiabatic system for different initial temperatures.
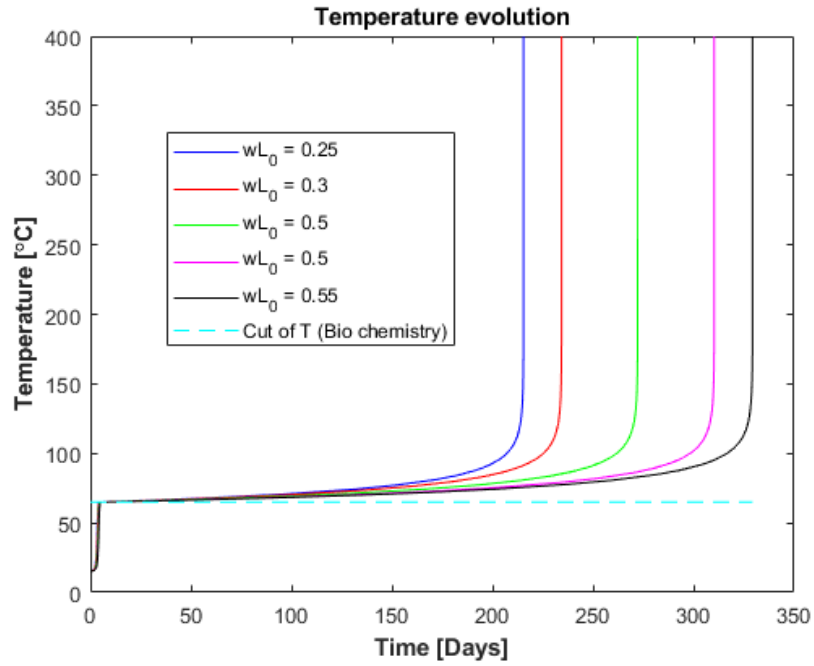
Figure 4.6: Temperature evolution in the adiabatic system for different initial moisture levels.
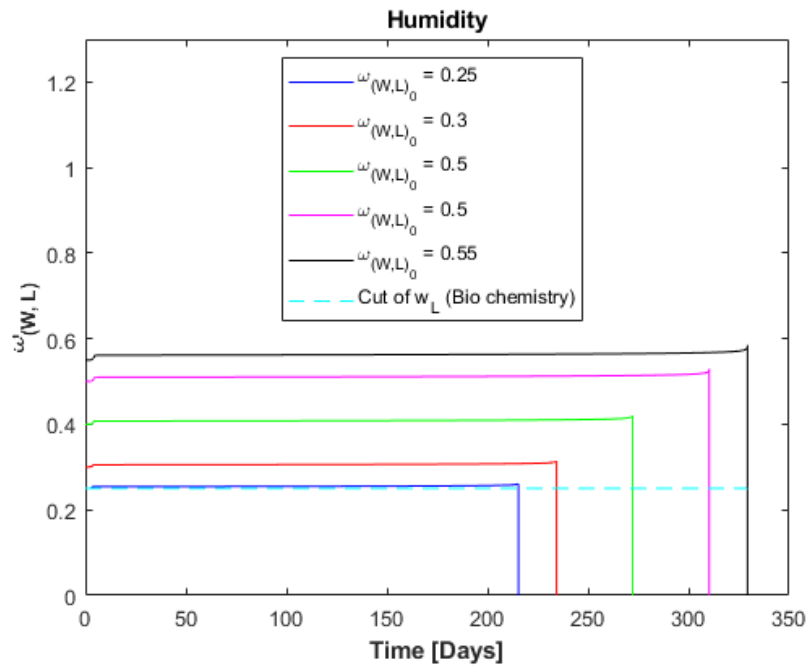
Figure 4.7: Time evolution of moisture level for the adiabatic system for different initial moisture levels in the substrate.
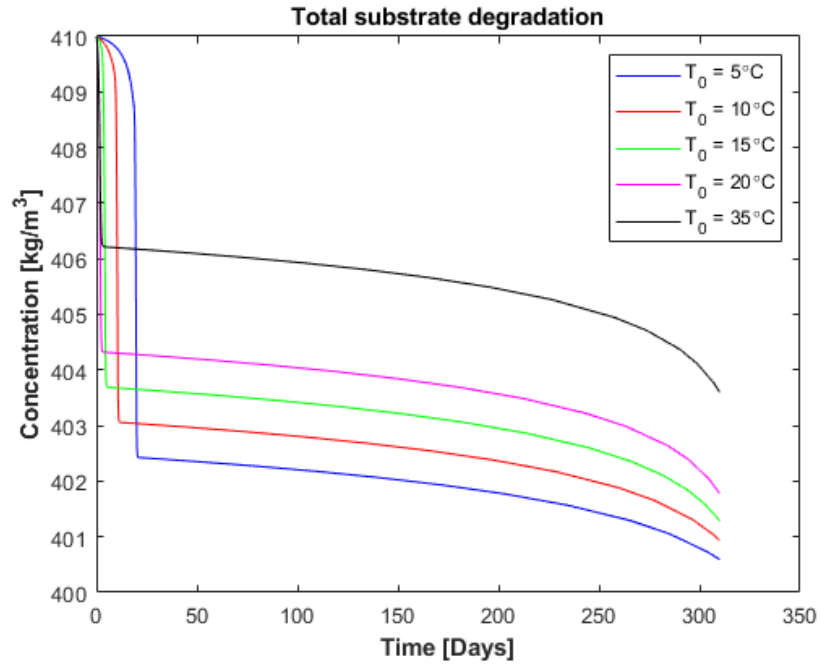
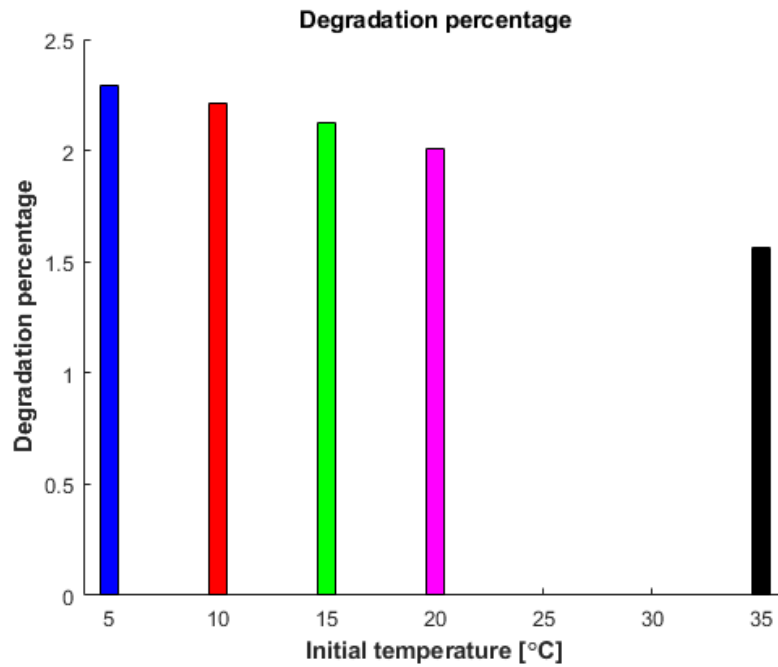Figure 4.8: Substrate degradation in the adiabatic system for different initial temperatures.

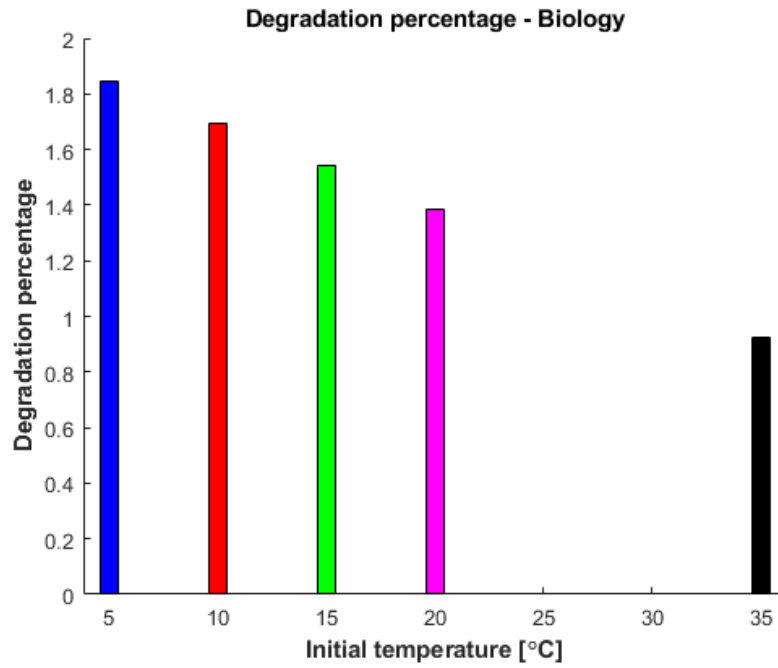Figure 4.9: Degradation percentage in the adiabatic system for different initial temperatures.

21

Figure 4.10: Percentage degraded by biological processes in the adiabatic system for different initial temperatures.

Chapter 5 - Future work

SLU togheter with Stockholm Exergi and other partners has an ongoing field study project in progress about biomass degradation. Among other quantities, temperature and gas emissions will be measured. These measurements will be going on in 2019-2020 at different locations in Sweden. It appears beneficial that both temperatures and emissions are being measured simultaneously since it makes it possible to correlate emissions to the different processes. The gases that I would suggest to measure in order to better understand mass loss and substrate degradation are carbon dioxide, carbon monoxide, methane and oxygen. Measuring the oxygen concentration in the stack will give information about how important anaerobic processes are to consider. Measuring gaseous concentrations could also provide information about how gases are transported inside the stack. Further research in literature is needed before adding transport to the model. To be able to asses the environmental impact of biomass storage emissions of sulfur oxide, hydrogen sulfide and laughing gas should also be measured.

Two approaches are suggested to increase the precision in the temperature interval between 65-80°C. The first approach would be to learn more about the biology in this temperature range. May the heat generation and material degradation be caused by thermophilic bacteria? Does the microorganisms die off with time once 65°C is reached? Here it could be a good idea to include a biochemist.

The second approach would be to perform long exposure oxidation experiments at constant temperature in a controlled lab environment. Equipment needed are a TGA-analysis which is to be coupled with a gas emission detector. Experiments should be performed at 80°C under both nitrogen and oxygen atmospheres and go on for at least a week. These measurements would yield information about how degradation depends on the partial pressure of oxygen and which products are formed during different atmospheres. Also detectable if any, degradation rate changes due to mechanical changes in the wood caused by low temperature oxidation. However, here there are some challenges that need to be considered. Chemical oxidation in low temperatures is slow, therefore it may be hard to detect emissions. One solution could be to perform these experiments in a closed system in which the gases would accumulate.

Chapter 6 - Conclusions

Aerobic processes in the pile consumes oxygen to degrade dry matter and produce heat. The initial oxygen concentration in air trapped in the stack is too low to facilitate significant losses and heat generation. Oxygen transport into the stack is thus vital to predict storage behaviour. Biological processes are known to control dry matter degradation at temperatures below 65°C while chemical oxidation reactions control the losses at elevated temperatures above 80°C which is captured by the model. However, the model fails to accurately capture the interplay between these processes in the temperature range between 65-80°C, leading to inaccurate predictions of thermal runaway and dry matter losses.

The temperature reaches 65°C in an isolated adiabatic system with an unlimited supply of oxygen within 2 to 20 days, depending on the initial temperature. The degradation of biomass within this time window is between 1.0-1.8%. This is significantly lower than the dry matter losses observed in the stacks in the field. The deviation is explained by heat transfer to the environment which keeps the temperature below 65°C for a longer time which allows the microorganisms to degrade more wood.

Chapter 7 - Appendices

7.1 Appendix A - Biological degradation

Evaluation of the biodegradation sub model.

7.1.1 Dry matter degradation

Ferrero et al. [23] created a modeled which considered an easily degradable fraction (S_E) and a slowly degradable fraction (S_H) and such a model was examined within this thesis. The model assumes that both the hard and easy fractions are consumed by microorganisms (m). The substances that are hard to degrade is through enzyme reactions turned into easy degradable substances. The extractives are partly consumed to grow new microorganisms and partly oxidized through metabolism. The degradation of solid material therefore occurs according to the system below:

$$\dot{\rho}_{S_H} = -r_1 \tag{7.1}$$

$$\dot{\rho}_{S_E} = r_1 - r_2 \tag{7.2}$$

$$\dot{\rho}_m = \alpha_1 r_2 - r_3 \tag{7.3}$$

$$r_1 = -\frac{k_1 \rho_{S_H}}{K_{S_1} \rho_m + \rho_{S_H}} \rho_m \tag{7.4}$$

$$r_2 = \frac{k_2 \rho_{S_E}}{K_{S_2} + \rho_{S_E}} \rho_m \tag{7.5}$$

$$r_3 = k_3 \rho_m \tag{7.6}$$

Where r_i denotes reaction rate and α_1 represents the mass fraction that is used to grow new microorganisms. The reaction rates r_1 and r_2 are based on Monod-kinetics which are a widely used within the framework of bio degradation. Table 7.1 shows a sample of paramters from Ferrero et al. [23]

Table 7.1: A sample of parameters from Ferrero et al. [23]

$k_1\ [s^{-1}]$	$k_2\ [s^{-1}]$	$k_3\ [s^{-1}]$	K_{S_1}	$K_{S_2}\ \left[\frac{kg}{m^3}\right]$	$\rho_{m0}\ \left[\frac{kg}{m^3}\right]$
$4.244 \cdot 10^{-5}$	$7.094 \cdot 10^{-5}$	$2.755 \cdot 10^{-5}$	6.5	$9.317 \cdot 10^{-3}$	$3.45 \cdot 10^{-2}$

Stability analysis

It is reasonable to assume that the degradation in equation 7.1 is slower than the degradation in equation 7.2. Hence, Investigations of the initial fast process governed by equations 7.2 and 7.3 was made by assuming the hard degradable fraction to be constant. The quasi-steady state (QSS) of the remaining two equations could readily be studied. Setting equation 7.2 and 7.3 to zero and solving for the densities of microorganisms and easily degradable substances yields in the following expressions:

$$\rho_m = \frac{1}{K_{S_1}} \left(-\rho_{S_H} + \frac{k_1 \rho_{S_H} (K_{S_2} + \rho_{S_E})}{k_2 \rho_{S_E}} \right) \tag{7.7}$$

$$\rho_{S_E} = \frac{k_3 K_{S_2}}{\alpha_1 k_2 - k_3} \tag{7.8}$$

Equation 7.7 gives quasi-steady-state values for the easy degradable fraction while equation 7.8 gives the quasi-steady-state value for the microorganisms. The intersection of the two functions determines the possible QSS states of the system. The QSS value of the microorganisms is obtained by substituting equation 7.8 into equation 7.8 resulting in the following point:

$$\rho_{S_E}^0 = \frac{k_3 K_{S_2}}{\alpha_1 k_2 - k_3}, \ \rho_m^0 = \frac{\rho_{S_H}(\alpha_1 k_1 - k_3)}{k_3 K_{S_1}} \tag{7.9}$$

Here it can be observed that the fast process have a quasi-steady sate in the first quadrant of the phase plane depicted in figure 7.1 if the following two conditions are satisfied:

$$\alpha_1 k_2 > k_3, \ \alpha_1 k_1 > k_3 \tag{7.10}$$

To ensure that these conditions are satisfied α_1 was taken as 0.68 which is the biomass yield coefficient reported by Ferrero et al. [23]. The stability of the reduced fast system was analyzed by studying how the system behaves when deviated QSS. This was done both qualitatively and by linearizing the system at the QSS point. Figure 7.1 shows the phase plane of the fast system given by equations 7.2 and 7.3. Figure 7.1 qualitatively shows how the system operates when deviated from the QSS point.
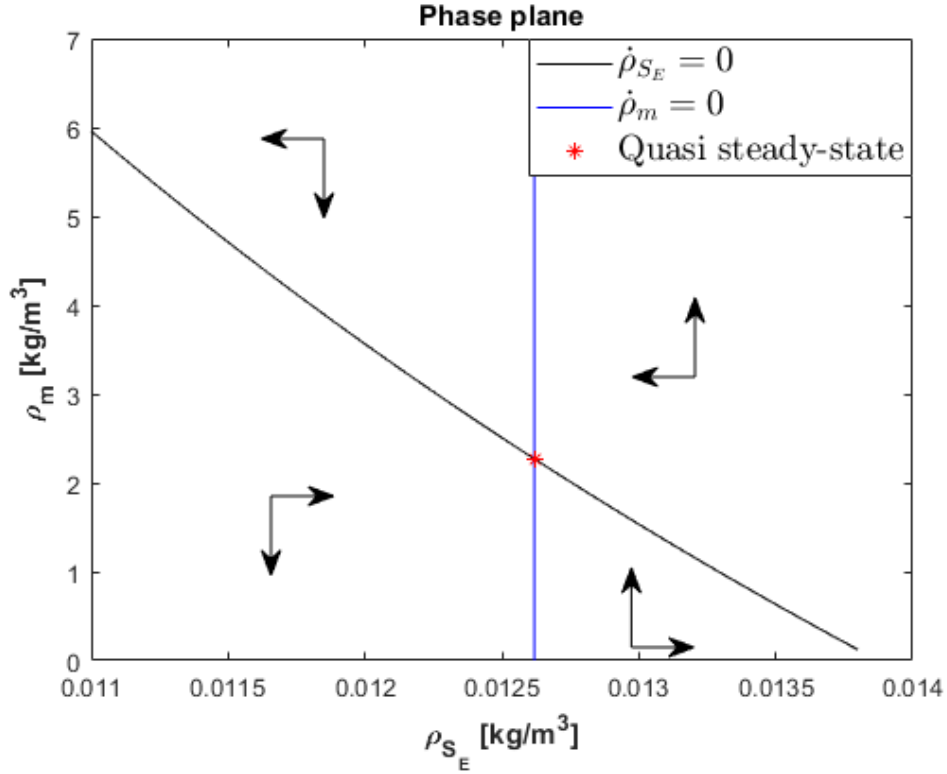
Figure 7.1: The arrows qualitatively show points trajectory in the plane.

Linearizing the system around the QSS gives information about the eigenvalues of the system which determines stability. For performing this analysis, let us rewrite the fast system given by equations 7.2 and 7.3 as:

$$\dot{\rho}_{S_E} = f(\rho_{S_E}, \rho_m) \tag{7.11}$$

$$\dot{\rho}_m = g(\rho_{S_E}, \rho_m) \tag{7.12}$$

Moving away from the steady-state.

$$\rho_{S_E} = \rho_{S_E}^0 + \Delta\rho_{S_E} \tag{7.13}$$

$$\rho_m = \rho_m^0 + \Delta\rho_m \tag{7.14}$$

Taking the derivative of 7.13 and 7.14.

$$\dot\rho_{S_E} = \frac{d}{dt}(\rho_{S_E}^0 + \Delta\rho_{S_E}) = \Delta\dot\rho_{S_E} \tag{7.15}$$

$$\dot\rho_m = \frac{d}{dt}(\rho_m^0 + \Delta\rho_m) = \Delta\dot\rho_m \tag{7.16}$$

Applying Taylor expansions.

$$\begin{aligned}\Delta\dot\rho_{S_E} &= f(\rho_{S_E}^0 + \Delta\rho_{S_E}, \rho_m^0 + \Delta\dot\rho_m) \\ &\approx f(\rho_{S_E}^0, \rho_m^0) + f_{\rho_{S_E}}(\rho_{S_E}^0, \rho_m^0)\Delta\rho_{S_E} + f_{\rho_m}(\rho_{S_E}^0, \rho_m^0)\Delta\rho_m\end{aligned} \tag{7.17}$$

$$\begin{aligned}\Delta\dot\rho_m &= g(\rho_{S_E}^0 + \Delta\rho_{S_E}, \rho_m^0 + \Delta\dot\rho_m) \\ &\approx g(\rho_{S_E}^0, \rho_m^0) + g_{\rho_{S_E}}(\rho_{S_E}^0, \rho_m^0)\Delta\rho_{S_E} + g_{\rho_m}(\rho_{S_E}^0, \rho_m^0)\Delta\rho_m\end{aligned} \tag{7.18}$$

This results in the following linearized system:

$$\Delta\dot\rho_{S_E} = f_{\rho_{S_E}}(\rho_{S_E}^0, \rho_m^0)\Delta\rho_{S_E} + f_{\rho_m}(\rho_{S_E}^0, \rho_m^0)\Delta\rho_m \tag{7.19}$$

$$\Delta\dot\rho_m = g_{\rho_{S_E}}(\rho_{S_E}^0, \rho_m^0)\Delta\rho_{S_E} + g_{\rho_m}(\rho_{S_E}^0, \rho_m^0)\Delta\rho_m \tag{7.20}$$

Taking the deriviatives of 7.2-7.3.

$$\begin{aligned}\Delta\dot\rho_{S_E} &= \left(\frac{k_2\rho_{S_E}^0\rho_m^0}{(K_{S_2} - \rho_{S_E}^0)^2} - \frac{k_2\rho_m^0}{K_{S_2} + \rho_{S_E}^0} \right)\Delta\rho_{S_E} \\ &+ \left(\frac{k_1\rho_{S_H}}{K_{s_1}\rho_m^0 + \rho_{S_H}} - \frac{k_1\rho_{S_H}K_{S_1}\rho_m^0}{(K_{s_1}\rho_m^0 + \rho_{S_H})^2} - \frac{k_2\rho_{S_E}^0}{K_{S_2} + \rho_{S_E}^0} \right)\Delta\rho_m\end{aligned} \tag{7.21}$$

$$\Delta\dot\rho_m = \left(\frac{\alpha_1 k_2\rho_m^0}{K_{S_2} + \rho_{S_E}^0} - \frac{\alpha_1 k_2\rho_{S_E}^0\rho_m^0}{(K_{S_2} + \rho_{S_E}^0)^2} \right)\Delta\rho_{S_E} + \left(\frac{\alpha_1 k_2\rho_{S_E}^0}{K_{S_2} + \rho_{S_E}^0} - k_3 \right)\Delta\rho_m \tag{7.22}$$

Plugging in the values from table 7.1 gives:

$$\Delta\dot\rho_{S_E} = -31 \cdot 10^{-3}\Delta\rho_{S_E} - 1.5685 \cdot 10^{-6}\Delta\rho_m \tag{7.23}$$

$$\Delta\dot\rho_m = 21 \cdot 10^{-3}\Delta\rho_{S_E} + 0 \cdot \Delta\rho_m \tag{7.24}$$

A stable steady-state has negative eigenvalues, the system is therefore expected to converge towards steady-state through 7.23. This was shown numerically in figure 7.2.
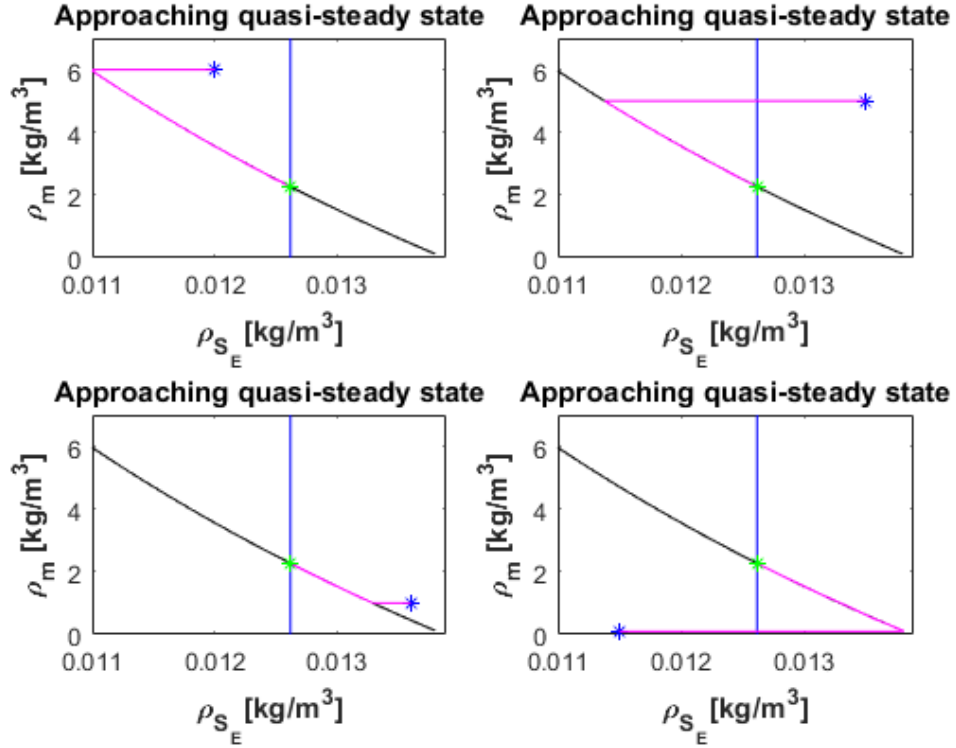
Figure 7.2: The figure illustrates how the reduced system with a constant value of the slowly degradable fraction approaches quasi-steady state. The blue star show the initial value, the pink curve shows the trajectory and the green star shows the final value.

Dynamics

It's of interest to know how the reaction rates r_1 and r_2 behaves. This is illustrated in figures 7.3-7.4. These figures show that the reaction rates may be simplified to $k_1\rho_m$ and $k_2\rho_m$ when ρ_{S_E} and ρ_{S_H} are not to close to zero, which is the initial case. These simplifications leads to the following system:

$$\dot{\rho}_{S_H} = -k_1\rho_m \tag{7.25}$$

$$\dot{\rho}_{S_E} = k_1\rho_m - k_2\rho_m \tag{7.26}$$

$$\dot{\rho}_m = \alpha_1 k_2\rho_m - k_3\rho_m \tag{7.27}$$

which has the following analytic solutions with the initial conditions $\rho_{S_H}(0) = \rho_{S_{H0}}$, $\rho_{S_E}(0) = \rho_{S_{E0}}$, $\rho_m(0) = \rho_{m0}$.

$$\rho_{S_H} = \rho_{S_{H0}} - \frac{-k_1}{\alpha_1 k_2 - k_3}\rho_{m_0}(e^{(\alpha_1 k_2 - k_3)t} - 1) \tag{7.28}$$

$$\rho_{S_E} = \rho_{S_{E0}} + \frac{k_2 - k_3}{\alpha_1 k_2 - k_3}\rho_{m_0}(e^{(\alpha_1 k_2 - k_3)t} - 1) \tag{7.29}$$

$$\rho_m = \rho_{m_0}e^{(\alpha_1 k_2 - k_3)t} \tag{7.30}$$

As, mentioned this simplified system is only valid before the easy fraction is heavily consumed. These analytic solutions show that the duration of the fast process depends on the initial condition of microorganisms which

is to be expected. The full time dependent system was thereafter integrated numerically. Solutions are shown in figure 7.5 and figure 7.6
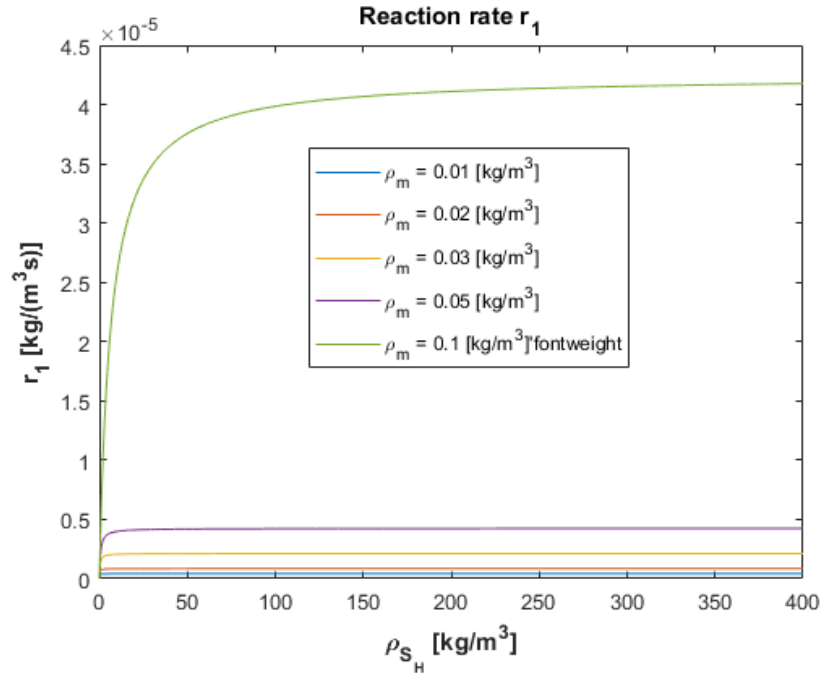

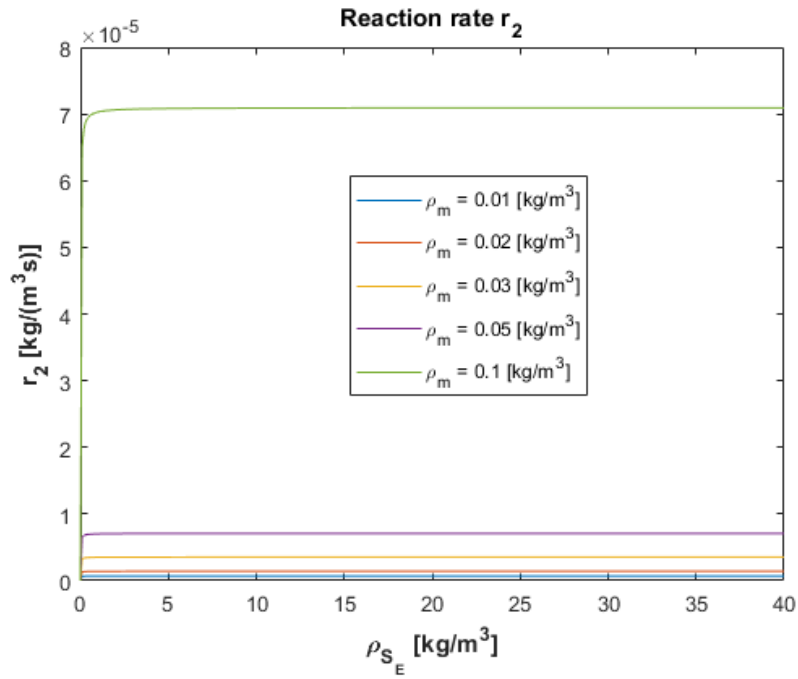Figure 7.3: Reaction rate r_1 at different concentrations of microorganisms

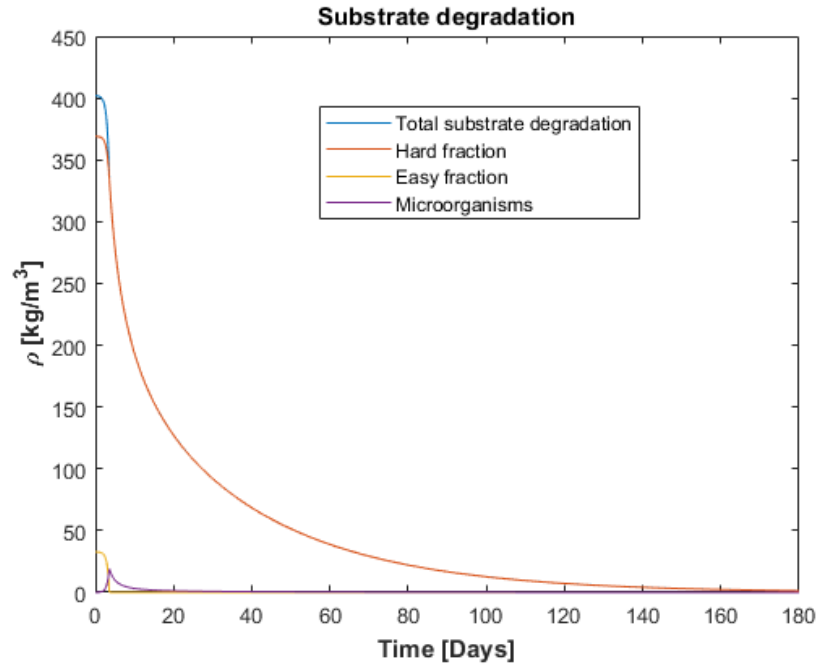Figure 7.4: Reaction rate r_2 at different concentrations of microorganisms

Figure 7.5: Substrate degradation obtained from numerical integration of equations 7.1-7.3. Initial conditions are $\rho_{S_H} = 369$ $[kg/m^3]$ and $\rho_{S_E} = 32.8$ $[kg/m^3]$ and $\rho_m = 3.45 \cdot 10^{-2}$ $[kg/m^3]$
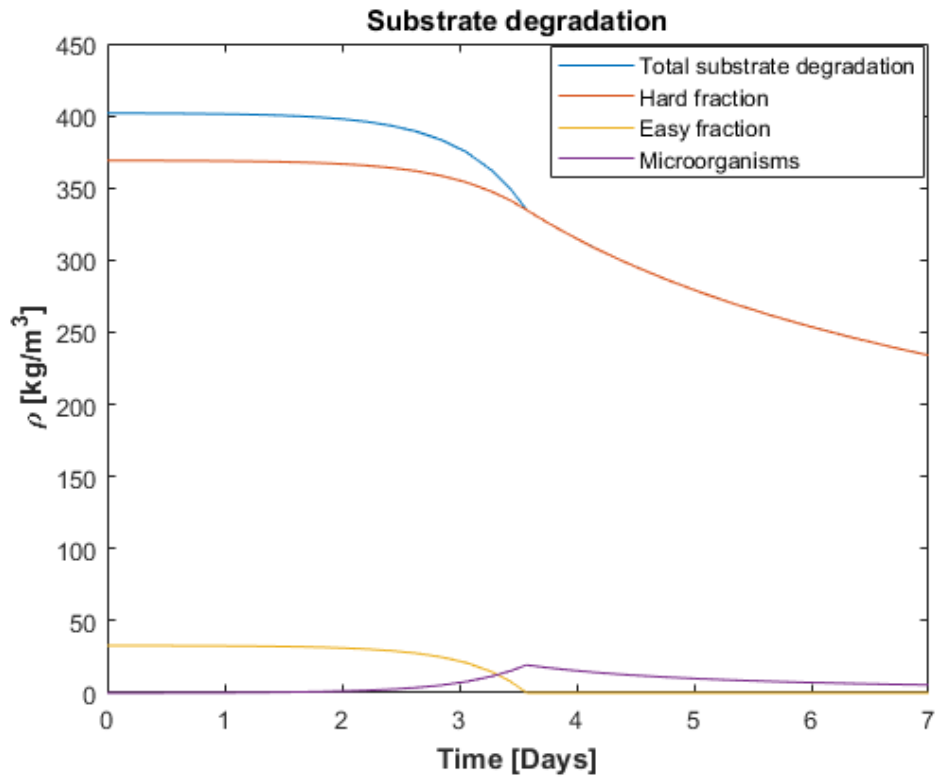
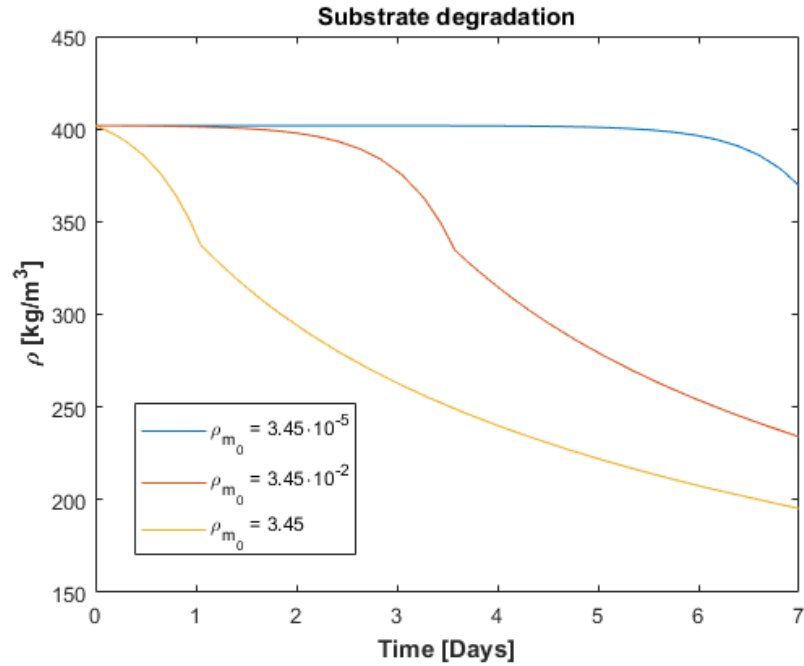Figure 7.6: Reprint of the data from figure 7.5 highlighting the first week.

Figure 7.7: Total substrate degradation profiles obtained from the integration of equations 7.1-7.3 for different initial microorganism concentrations. Initial conditions are $\rho_{S_H} = 369 \ [kg/m^3]$ and $\rho_{S_E} = 32.8 \ [kg/m^3]$.
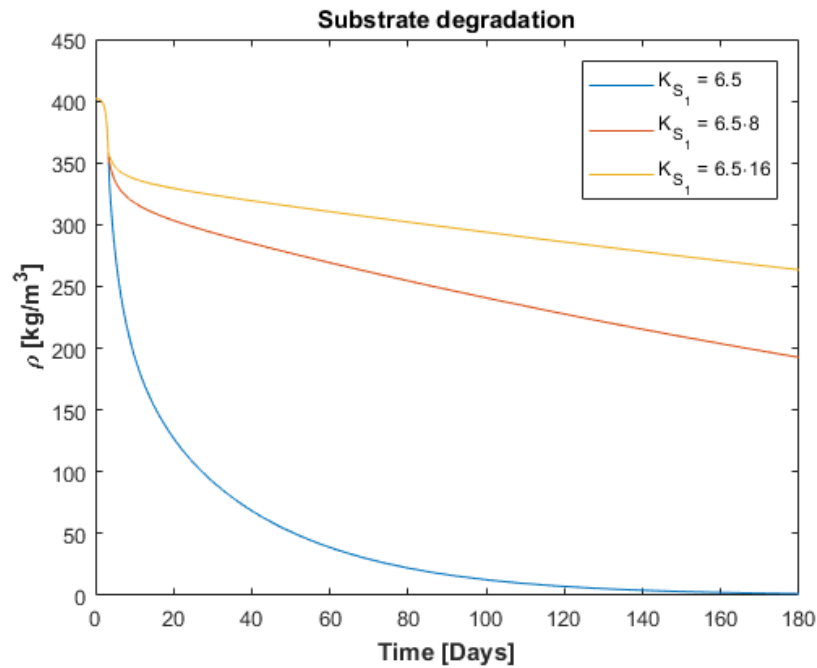

Figure 7.8: Total substrate degradation profiles obtained from the integration of equations 7.1-7.3 for varying values of K_{S_1}. Initial conditions are $\rho_{S_H} = 369 \ [kg/m^3]$ and $\rho_{S_E} = 32.8 \ [kg/m^3]$ and $\rho_m = 3.45 \cdot 10^{-2} \ [kg/m^3]$

Figures 7.5 and 7.6 show that the degradation follows the expected route. An initial time scale where both the easily degradable substance and the hard to degrade substance are consumed followed by a degradation period solely controlled by the slow fraction. However, the density evolution does not completely match what is expected from literature. It can be concluded by studying the quasi-steady state point shown in expression 7.9 and the analytic solutions in equations 7.28-7.30 that the parameter K_{S_1} and the initial condition of microorganisms are suitable parameters to change to adjust the model. The initial concentration of microorganisms controls the fast process, while K_{S_1} controls the slow evolution. Figure 7.7 showcases how the initial degradation changes depending on the initial condition of microorganisms. Figure 7.8 illustrates how the second timescale changes with changing values of K_{S_1}.

7.1.2 Heat generation

The temperature evolution is governed by oxygen transport which makes it tricky to evaluate the heat generation without adding transport equations. An evaluation of the heat generation was done by considering the heat generated in a isolated system with an initial concentration of oxygen corresponding to the value in air. The density of the dry matter and the moisture content was kept constant during this estimation. The oxygen concentration in air, modeled as an ideal gas at normal temperature and pressure, is 8.73 mol O_2/m^3 on dry air basis. The temperature increase resulting from microbial activity is expressed in equation 7.31. Table 7.2 shows parameter values used to calculate heat generation.

$$\Delta T = -\frac{\Delta H_C}{\rho c_p} n_{CO_2} \tag{7.31}$$

Table 7.2: Values used to evaluate heat generation by microbial activity.

ΔH_C $\left[\frac{kJ}{mol\ CO_2}\right]$ [3]	$C_{p_{DM}}$ $\left[\frac{kJ}{kgK}\right]$ [22]	C_{pw} $\left[\frac{kJ}{kgK}\right]$	ρ_{DM} $\left[\frac{kg}{m^3}\right]$ [22]	$\rho\ (\omega_{(W,L)} = 0.55)$ $\left[\frac{kg}{m^3}\right]$
1100	1.3	4.18	410	635.5

The heat capacity is expressed by equation 7.32.

$$c_p = \frac{C_{p_{(W,L)}}\omega_{(W,L)} + C_{p_{DM}}}{(1 + \omega_{(W,L)})} \tag{7.32}$$

Where $\omega_{(W,L)}$ is the weight fraction of water on dry basis. It is apparent from the values displayed in table 7.2 that the moisture content within the substrate affects the heating rate. A moisture content of 55 wt% yields in a temperature increase of 4.81 K while the temperature increase is 18.02 K for dry wood.

7.2 Appendix B - Chemical oxidation

Evaluation of the chemical oxidation sub model.

7.2.1 Material degradation

The substrate degradation by chemical oxidation was modeled as a first order reaction with respect to the degradable fractions of the substrate concentration:

$$\dot{\rho}_S = -(\rho_{S_H} + \rho_{S_E})k_0 e^{(-E_A/(RT))} g_2(O_2) \tag{7.33}$$

The analytic solution to equation 7.33 is expressed below.

$$\rho_S(t) = (\rho_{S_H} + \rho_{S_E})_0 e^{-\beta t} \tag{7.34}$$

$$\beta = k_0 e^{(-E_A/(RT))} g_2(O_2) \tag{7.35}$$

Where $\rho_S = \rho_{S_H} + \rho_{S_E}$

Table 7.3: Kinetic parameters from Ferrero et al. [23]

$k_0 \ [s^{-1}]$	$E_A/R \ [K]$
$8.15 \cdot 10^5$	12.509

Table 7.3 shows kinetic oxidation parameters used by Ferrero et al. [23] These parameters have been used in equation 7.34 to produce figure 7.9. Figure 7.9 shows solutions at constant temperatuares of 120°C and 200°C.
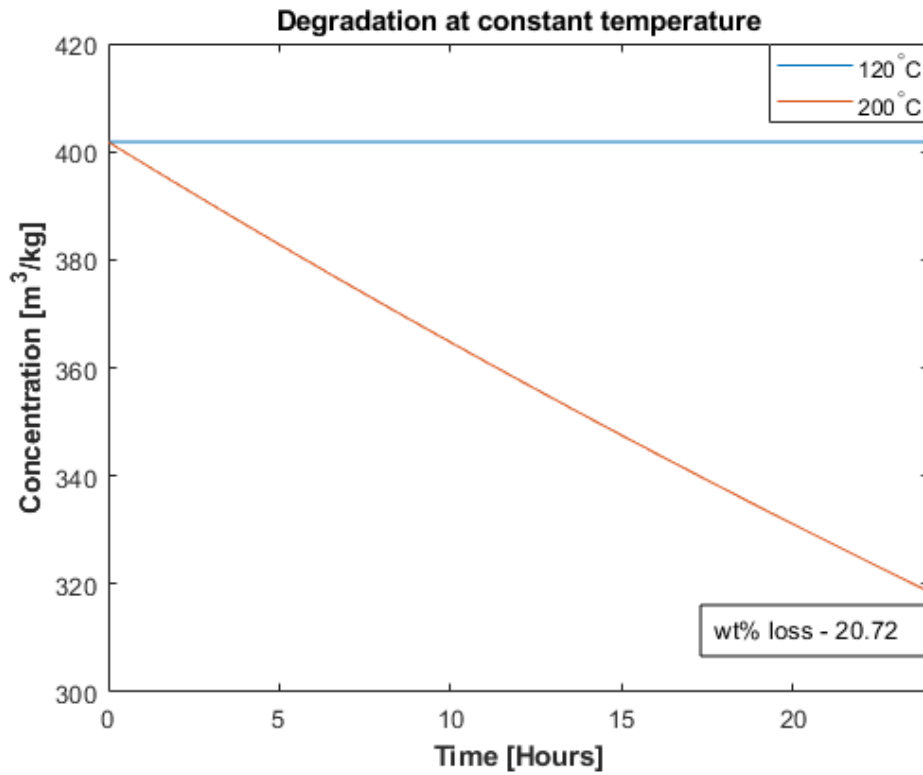

Figure 7.9: Degradation by chemical oxidation at constant temperature.

Figure 7.9 shows that the degradation by chemical oxidation during 24 hours, with parameter values form Ferrero et al. [23], is in the accepted magnitude.

7.3 Appendix C - Physical transformation

The physical transformation was approached by assuming that the atmosphere inside the stack is saturated with water vapor. Assuming saturated vapor means that the vapor pressure is a function of temperature. In this work the empirical function shown below has been used to calculate the saturation pressure.

$$\log p_{(W,V)} = A - \frac{B}{T+C} \tag{7.36}$$

This function was tested against tabulated data from *Tabeller och diagram för energitekniska beräkningar* [30]. The result is shown in figure 7.10.
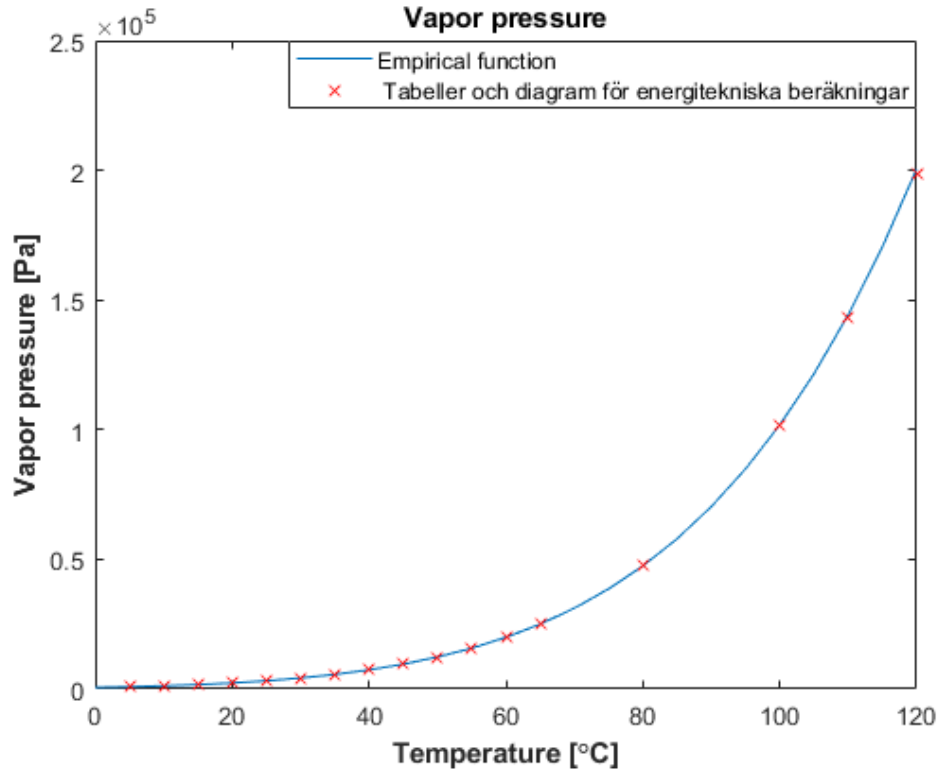

Figure 7.10: Vapor pressure versus temperature both calculated values and tabulated values are shown.

Once the saturation pressure is given, the density of water vapor may be expressed by the ideal gas law.

$$\rho_{(W,V)}(T) = \exp\left(A - \frac{B}{T+C}\right)\frac{M_{H_2O}}{RT}f\epsilon \tag{7.37}$$

Here, f is an conversion factor that converts the pressure to Pa and weight to kg while ϵ describes the porosity of the pile. It is of interest to see in which magnitude the vapor density is at in the temperature range between 0-100°C since the model assumes saturated water vapor. If the values of vapor density are relative low compared to the initial concentration of liquid water the assumption holds for a large temperature range. The density evolution with temperature is shown in figure 7.11
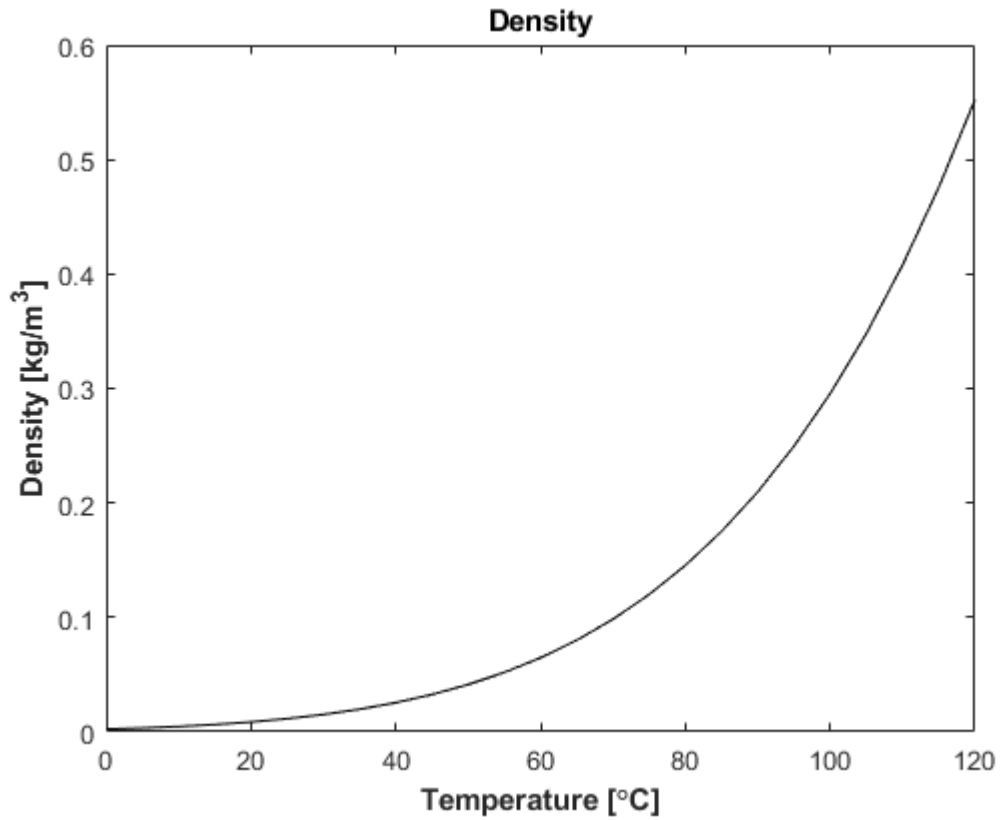
Figure 7.11: Density of water vapor at saturated conditions.

Figure 7.11 shows that the saturation density is well below the 225.5 kg/m^3 which is the initial condition of liquid water inside the stack. This indicates that the model may hold for a long time. Transport phenomena must be included to determine how long it takes before the stack is dried out.

7.4 Appendix D - All processes

This appendix accounts for the derivation of the temperature evolution with time. See the previous appendixes for information about reaction rates etc.

7.4.1 Energy balance

The system – the control volume

Volume: $\sim 10^{-2}\ [m]$

Bio-chemical reactions
Chemical oxidation reactions
Evaporation/condensation of water

$$F = F_{out} - F_{in} \left[\frac{kg}{s}\right]$$

$$Q\left[\frac{kJ}{m^3 s}\right]$$

Black – inflow (mass)
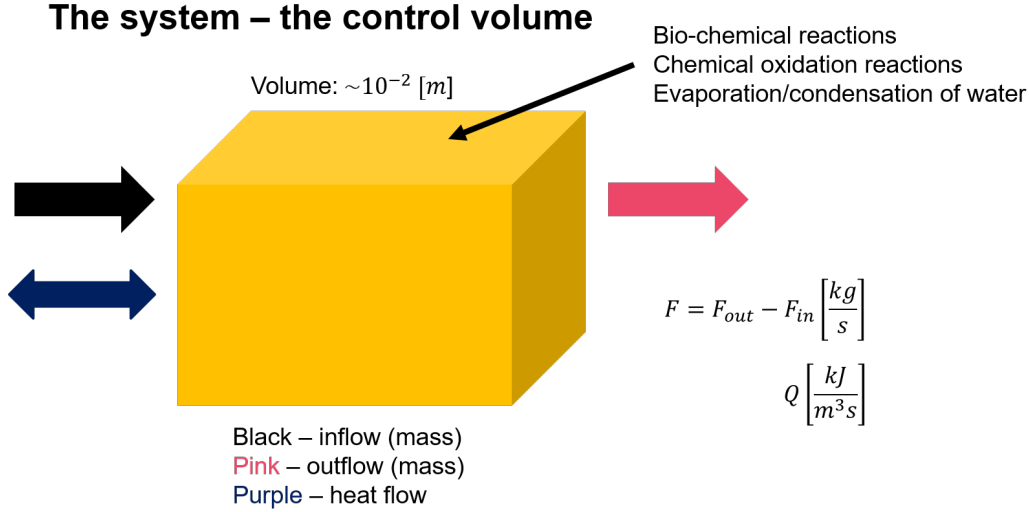Pink – outflow (mass)
Purple – heat flow

Figure 7.12: Caption

Let us consider a homogeneous domain with volume V. Starting from the mass balances which includes biochemical reactions (green), chemical oxidation reactions (red), physical transformation of water (blue) as well as transport (black). Transport is only considered for gaseous species.

$$\dot{\rho}_{S_H} = -r_1 - \frac{\rho_{S_H}}{\rho_{S_H} + \rho_{S_E}} r_4 \tag{7.38}$$

$$\dot{\rho}_{S_E} = r_1 - r_2 - \frac{\rho_{S_E}}{\rho_{S_H} + \rho_{S_E}} r_4 \tag{7.39}$$

$$\dot{\rho}_{S_I} = 0 \tag{7.40}$$

$$\dot{\rho}_m = \alpha_1 r_2 - r_3 \tag{7.41}$$

$$\dot{\rho}_d = r_3 \tag{7.42}$$

$$\dot{\rho}_{(W,V)} = \frac{dT}{dt}\frac{d\rho_{(W,V)}}{dT} \tag{7.43}$$

$$\dot{\rho}_{O_2} = -6\alpha_2\frac{M_{O_2}}{M_{S_E}} r_2 - \nu_1\frac{M_{O_2}}{M_S} r_4 - \frac{F_{O_2}}{V} \tag{7.44}$$

$$\dot{\rho}_{CO_2} = 6\alpha_2\frac{M_{CO_2}}{M_{S_E}} r_2 + \nu_2\frac{M_{CO_2}}{M_S} r_4 - \frac{F_{CO_2}}{V} \tag{7.45}$$

$$\dot{\rho}_{(W,L)} = -\dot{\rho}_{(W,V)} + 6\alpha_2\frac{M_{H_2O}}{M_{S_E}} r_2 + \nu_3\frac{M_{H_2O}}{M_S} r_4 - \frac{F_{W,V}}{V} \tag{7.46}$$

$$\dot{\rho}_{N_2} = -\frac{F_{N_2}}{V} \tag{7.47}$$

Where F_j refers to the mass flow out of the domain in kg/s. Here, $j = O_2$, N_2, CO_2 and *water vapor*.

The energy of the system may be expressed as:

$$H = \sum \rho_i h_i \left[\frac{kJ}{m^3} \right] \tag{7.48}$$

The time evolution becomes

$$\frac{dH}{dt} = \frac{d}{dt}\left(\sum \rho_i h_i \right) = \left(\frac{d\rho_i}{dt} h_i + \rho_j \frac{dh_j}{dt} \right) + ... + \left(\frac{d\rho_i}{dt} h_n + \rho_n \frac{dh_n}{dt} \right) \tag{7.49}$$

Which is equal to the energy that is transferred with the system and its surroundings.

$$\frac{dH}{dt} = Q - \frac{F_{N_2} h_{N_2} + F_{O_2} h_{O_2} + F_{CO_2} h_{CO_2} + F_{(W,V)} h_{(W,V)}}{V} \tag{7.50}$$

Where Q is the heat flow per unit volume into the domain.

The second term in equation 7.49 was treated in the following fashion:

$$\frac{dh_i}{dt} = \frac{dh_i}{dT} \frac{dT}{dt} = c_{p,i} \frac{dT}{dt} \tag{7.51}$$

Combining the mass balances with equations 7.49 to 7.51 yields in the following expression:

$$
\begin{aligned}
Q &- \frac{F_{N_2} h_{N_2} + F_{O_2} h_{O_2} + F_{CO_2} h_{CO_2} + F_{(W,V)} h_{(W,V)}}{V} = r_1 (h_{S_E} - h_{S_H}) \\
&+ r_2 \left(6\alpha_2 \frac{M_{H_2O}}{M_{S_E}} h_{(W,L)} + 6\alpha_2 \frac{M_{CO_2}}{M_{S_E}} h_{CO_2} - 6\alpha_2 \frac{M_{O_2}}{M_{S_E}} h_{O_2} - h_{S_E} + \alpha_1 h_m \right) + r_3 (h_d - h_m) \\
&+ r_4 \left(-\nu_1 \frac{M_{O_2}}{M_S} h_{O_2} + \nu_2 \frac{M_{CO_2}}{M_S} h_{CO_2} + \nu_3 \frac{M_{H_2O}}{M_S} h_{(W,L)} - \frac{\rho_{S_H}}{\rho_{S_H} + \rho_{S_E}} h_{S_H} - \frac{\rho_{S_H}}{\rho_{S_E} + \rho_{S_E}} h_{S_E} \right) \\
&- \frac{F_{N_2} h_{N_2} + F_{O_2} h_{O_2} + F_{CO_2} h_{CO_2} + F_{(W,V)} h_{(W,L)}}{V} + \sum C_{p,i} \rho_i \frac{dT}{dt} + \frac{dT}{dt} \frac{d\rho_{W,V}}{dT} \Delta H_{Vap}
\end{aligned}
\tag{7.52}
$$

Rearranging for temperature and assuming that the energy transformation is neglectable when the hard fraction is turned into the easy fraction as well as when the active microorganism dies results in the final expression shown below:

$$
\dot{T} = \frac{Q - \frac{F_{(W,V)}}{V} \Delta H_{Vap} - 6\alpha_2 \frac{M_{CO_2}}{M_{S_E}} \Delta H_R r_2 - \Delta H_C r_4}{\sum \rho_i c_{p,i} + \frac{d\rho_{(W,V)}}{dT} \Delta H_{Vap}}
$$

$$Where$$

$$-6\alpha_2 \frac{M_{CO_2}}{M_{S_E}} \Delta H_R = 6\alpha_2 \frac{M_{H_2O}}{M_{S_E}} h_{(W,L)} + 6\alpha_2 \frac{M_{CO_2}}{M_{S_E}} h_{CO_2} - 6\alpha_2 \frac{M_{O_2}}{M_{S_E}} h_{O_2} - h_{S_E} + \alpha_1 h_m$$

$$-\Delta H_C = -\nu_1 \frac{M_{O_2}}{M_S} h_{O_2} + \nu_2 \frac{M_{CO_2}}{M_S} h_{CO_2} + \nu_3 \frac{M_{H_2O}}{M_S} h_{(W,L)} - \frac{\rho_{S_H}}{\rho_{S_H} + \rho_{S_E}} h_{S_H} - \frac{\rho_{S_H}}{\rho_{S_E} + \rho_{S_E}} h_{S_E}$$

$$\tag{7.53}$$

7.5 Case 2

The energy that is required to heat a system is decided by the amount of mass and the heating values of the individual materials. In the second case an endless depot of oxygen is simulated by asserting the value 1 to the dependency function $g_2(O_2)$ at all times while keeping the initial value of oxygen to that in air. This presents a inaccuracy since the models built up carbon dioxide while assigning negative values of oxygen. The density of carbon dioxide increases faster than the density of oxygen goes away since the molecular wight is higher for carbon dioxide. Here, there is an increase in gases species which means that more energy

has to be added to heat up the system than in a real scenario. The magnitude of this error was investigated here. Consider the case in which the initial temperature is 15°C. The initial value of $\rho_{O_2} c_{p_{O_2}} + \rho_{CO_2} c_{p_{CO_2}}$ is 0.12 kJ/(m$^3 \cdot$ K). After 310 days of storage the value have increased to 1.02 kJ/(m$^3 \cdot$ K). The initial value of $\rho_{DM} c_{DM}$ is 533 kJ/(m$^3 \cdot$ K), the value decreases to 524.68 kJ/(m$^3 \cdot$ K) after 310 days of storage. The error discussed here is negligible since $524.68 \gg 1.02$.
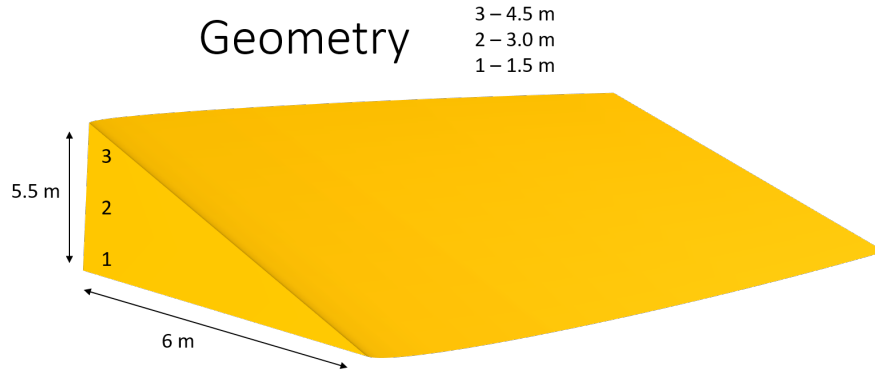
Figure 7.13: Dimensions of the piles as well as measured positions within the piles.

7.6 Appendix E - Field study result

The experimental data presented here is from a field study performed at Nykvarn, Sweden between February to August in 2017. The study was conducted by Erik Anerud from SLU. Here, data is shown from two stacks. One of these stack were covered while the other one was kept uncovered. These stacks were composed of stemwood and they were built against a wall, the maximum height of the piles were 5.5 m. Measurements are shown from three different positions within the piles. The first position had a height of 1.5 m, the second was placed 3.0 m above the ground and the third position had a height of 4.5 m. The piles and the positions are illustrated in figure 7.13.

Figure 7.14 shows the percentage of degraded substrate after 30, 60, 120 and 180 days for the uncovered and covered pile. The shown data is produced by three sample points. The biggest degradation happened within the first 30 days of storage. Lower degradation percentages were measured in the covered pile compared to the uncovered pile. Generally, position 1 experienced the lowest degradation.

Figure 7.15 shows the moisture content of the wood i.e the weight fraction of liquid water after 0, 30, 60, 120 and 180 days of storage. Data is presented for the uncovered and covered pile. The initial data point for moisture was produced by 12 sample points while the rest were produced by three sample points. Here it can be seen that the moisture level varies less in the covered pile than in the uncovered pile. The initial moisture content were around 35 wt%. The fraction of liquid water never dropped below the fibre saturation point (25 wt%).

Figure 7.16 shows the temperature evolution in the stack during the first 30 days of storage as well as the ambient temperature during this time. The initial temperature was close to 47°C. Position 2 and 3 show greater increase in temperature than position 1. Data for position 1 is less consistent than for the other two positions. The temperature profile in position 2 and 3 are similar to each other. The lowest recorded temperature in position 3 was 9.9°C, this temperature was measured during day 29. The highest temperature in position 3 was recorded after 11 days of storage, the temperature reached 156.4°C. The lowest temperature in position 2 was measured to be 10.4°C after 24 days. The temperature reached its peak at 143°C during day 12 in position 2.

Figure 7.17 shows the ambient temperature and the temperature profile in the stack during the first 30 days of storage for the covered pile. The temperature profiles are similar in all three positions. The temperature fluctuates between 40-70°C in all three positions.
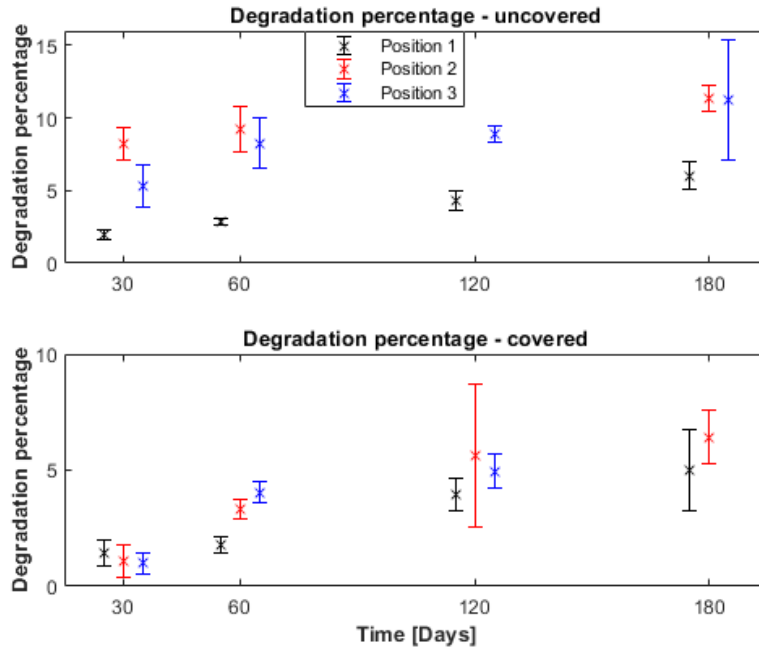
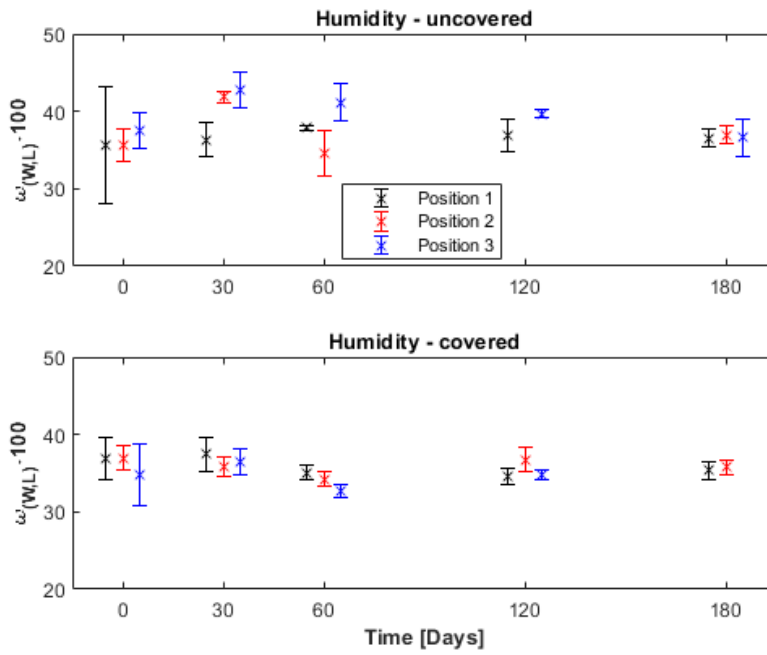Figure 7.14: Percentage of degraded biomass.

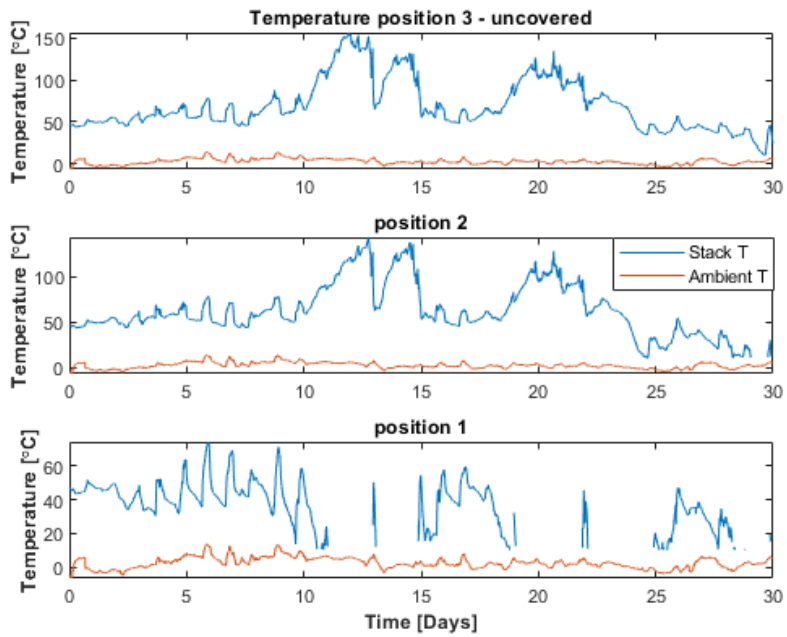Figure 7.15: The humidity inside the stacks.
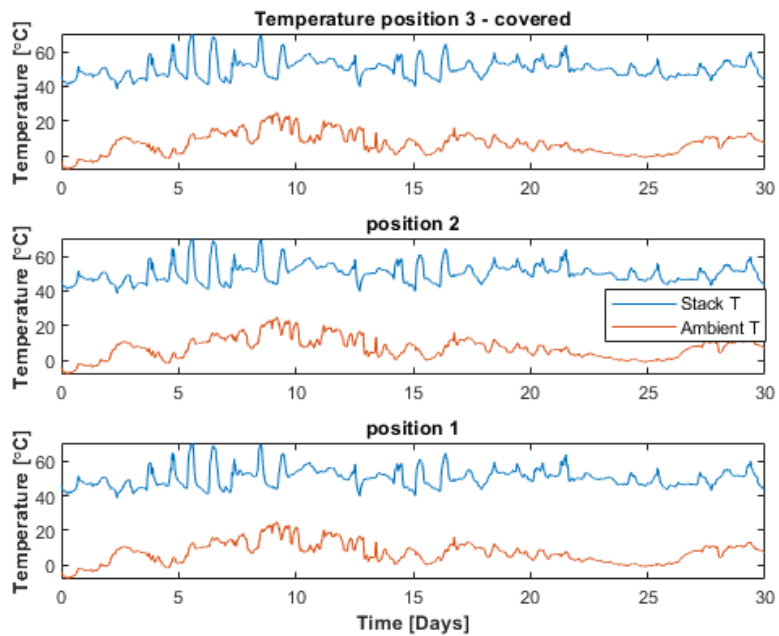
Figure 7.16: Temperature profiles in the uncovered stack.

Figure 7.17: Temperature profiles in the covered stack.

43

Bibliography

[1] Tore Filbakk et al. "Modelling moisture content and dry matter loss during storage of logging residues for energy". eng. In: *Scandinavian Journal of Forest Research* 26.3 (2011), pp. 267–277. ISSN: 0282-7581.

[2] *European Commission-2030 Energy Strategy - Energy*. en. URL: `/energy/en/topics/energy-strategy-and-energy-union/2030-energy-strategy` (visited on 02/05/2019).

[3] S. Krigstin and S. Wetzel. "A review of mechanisms responsible for changes to stored woody biomass fuels". In: *Fuel* 175 (2016), pp. 75–86. ISSN: 00162361.

[4] Vladimir Strezov and Tim J. Evans. *Biomass Processing Technologies*. eng. 1st ed. CRC Press, 2014. ISBN: 9781466566163.

[5] Muhammad T. Afzal et al. "STORAGE OF COMMINUTED AND UNCOMMINUTED FOREST BIOMASS AND ITS EFFECT ON FUEL QUALITY". eng. In: *BioResources* 5.1 (2010), pp. 55–69. ISSN: 1930-2126. URL: `https://doaj.org/article/d8e724daa1dc4cc488fa4e0c7bc32a6c`.

[6] Birgitta Strömberg and Solvie Herstad Svärd. *Bränslehandboken 2012*. 2012.

[7] A.A. Rentizelas. "6 - Biomass storage". eng. In: *Biomass Supply Chains for Bioenergy and Biorefining*. 2016, pp. 127–146. ISBN: 978-1-78242-366-9.

[8] Nicolas Hofmann et al. "Drying effects and dry matter losses during seasonal storage of spruce wood chips under practical conditions". eng. In: *Biomass and Bioenergy* 111 (2018), pp. 196–205. ISSN: 0961-9534.

[9] *Skånska dagbladet - Stor brand i flislager*. July 7, 2011. URL: `https://www.skd.se/2011/07/07/stor-brand-i-flislager/` (visited on 06/24/2019).

[10] Wallace E. Eslyn. "Evaluating Chemicals for Controlling Biodeterioration of Stored Wood Chips". In: *Forest Products Journal* 23.11 (1973), pp. 21–24.

[11] Gerd Wegener Dietrich Fengel. *Wood: Chemistry, ultrastructure, reactions*. eng ; deu. Originally published 1983 ; Im Original erschienen 1983. Berlin, New York: DE GRUYTER, 1983. ISBN: 978-3-11-008481-8.

[12] Olaf Schmidt. *Wood and Tree Fungi: Biology, Damage, Protection, and Use*. eng. Berlin, Heidelberg: Springer Berlin Heidelberg, 2006. ISBN: 978-3-540-32138-5.

[13] Yu Fukasawa. "Temperature effects on hyphal growth of wood-decay basidiomycetes isolated from Pinus densiflora deadwood". eng. In: *Mycoscience* 59.3 (2018), pp. 259–262. ISSN: 1340-3540.

[14] R. A. (Robert A.) Zabel. *Wood microbiology decay and its prevention*. eng. San Diego: Academic Press, Inc., 1992. ISBN: 0-323-13946-9.

[15] Märta-Lena Ernstson, Raída Jirjis, and Anders Rasmuson. "Experimental determination of the degradation rate for some forest residue fuel components at different temperatures and oxygen concentrations". In: *Scandinavian Journal of Forest Research* 6.1-4 (1991), pp. 271–287. DOI: 10.1080/02827589109382668. eprint: `https://doi.org/10.1080/02827589109382668`. URL: `https://doi.org/10.1080/02827589109382668`.

[16] *Methanogens - an overview — ScienceDirect Topics*. URL: `https://www.sciencedirect.com/topics/agricultural-and-biological-sciences/methanogens` (visited on 03/12/2019).

[17] F. Ferrero, M. Malow, and M. Noll. "Temperature and gas evolution during large scale outside storage of wood chips". eng ; ger. In: *European Journal of Wood and Wood Products* 69.4 (2011), pp. 587–595. ISSN: 0018-3768.

[18] Carly Whittaker et al. "Dry Matter Losses and Greenhouse Gas Emissions From Outside Storage of Short Rotation Coppice Willow Chip". eng. In: *BioEnergy Research* 9.1 (2016), pp. 288–302. ISSN: 1939-1234.

[19] Fred Shafizadeh. "Pyrolytic Reactions and Products of Biomass". In: *Fundamentals of Thermochemical Biomass Conversion*. Ed. by R. P. Overend, T. A. Milne, and L. K. Mudge. Dordrecht: Springer Netherlands, 1985, pp. 183–217. ISBN: 978-94-009-4932-4. DOI: 10.1007/978-94-009-4932-4_11. URL: https://doi.org/10.1007/978-94-009-4932-4_11.

[20] Evgeniya Popova et al. "Thermal degradation and combustion of wood fuels, coals and hydrolyzed lignin from the Russian Federation: experiments and modeling". In: *Bioresource Technology* 218 (July 2016), pp. 1046–1054. DOI: 10.1016/j.biortech.2016.07.033.

[21] M.A. Dietenberger and L.E. Hasburgh. "Wood Products: Thermal Degradation and Fire". eng. In: *Reference Module in Materials Science and Materials Engineering*. 2015, pp. 9712–9716. ISBN: 978-0-12-803581-8.

[22] Märta-Lena Ernstson and Anders Rasmuson. "Mathematical modelling of transport processes and degradation reactions in piles of forest fuel material". eng. In: *Fuel* 72.11 (1993), pp. 1515–1524. ISSN: 0016-2361.

[23] Fabio Ferrero et al. "A mathematical model to predict the heating-up of large-scale wood piles". eng. In: *Journal of Loss Prevention in the Process Industries* 22.4 (2009), pp. 439–448. ISSN: 0950-4230.

[24] Ulrich Krause, Martin Schmidt, and Christian Lohrer. "A numerical model to simulate smouldering fires in bulk materials and dust deposits". eng. In: *Journal of Loss Prevention in the Process Industries* 19.2 (2006), pp. 218–226. ISSN: 0950-4230.

[25] Ali Rostami, Jayathi Murthy, and Mohammad Hajaligol. "Modeling of smoldering process in a porous biomass fuel rod". eng. In: *Progress in Energy and Combustion Science* 83.11 (2004), pp. 1527–1536. ISSN: 0016-2361.

[26] Richard M Felder. *Elementary principles of chemical processes*. eng. 3. ed.. Hoboken, N.J.: Wiley, 2005. ISBN: 9780471375876Int.

[27] *COMSOL - Diffusion equation*. Accessed: 2019-06-02. URL: https://www.comsol.com/multiphysics/diffusion-equation.

[28] J. F Richardson et al. *Chemical Engineering Volume 2: Vol. 2,Particle technology and separation processes*. eng. 5th ed. Chemical Engineering Series 0. 2013. ISBN: 0750644451.

[29] *Natural convection and buoyancy driven flows - ANSYS*. Accessed: 2019-06-02. URL: https://www.sharcnet.ca/Software/Ansys/16.2.3/en-us/help/flu_ug/flu_ug_sec_hxfer_buoy.html.

[30] Lars Wester. *Tabeller och diagram för energiteksniska beräkningar*. swe. MARKLUND SOLUTIONS, 2015.